

We are IntechOpen, the world's leading publisher of Open Access books Built by scientists, for scientists

6,900

Open access books available

185,000

International authors and editors

200M

Downloads

Our authors are among the

154

Countries delivered to

TOP 1%

most cited scientists

12.2%

Contributors from top 500 universities



WEB OF SCIENCE™

Selection of our books indexed in the Book Citation Index
in Web of Science™ Core Collection (BKCI)

Interested in publishing with us?
Contact book.department@intechopen.com

Numbers displayed above are based on latest data collected.
For more information visit www.intechopen.com



Characterization and Modeling of Charging Effects in Dielectrics for the Actuation of RF MEMS Ohmic Series and Capacitive Shunt Switches

Romolo Marcelli et al.*
CNR-IMM Roma, Roma,
Italy

1. Introduction

Charge accumulation in dielectrics solicited by an applied voltage, and the associated temperature and time dependencies are well known in scientific literature since a number of years [1]. The potential utilization of materials being part of a device useful for space applications is a serious issue because of the harsh environmental conditions and the necessity of long term predictions about aging, out-gassing, charging and other characteristic responses [2], [3]. Micro-mechanical Systems (MEMS) for RF applications have been considered for sensor applications as well as for high frequency signal processing during more than one decade [4], [5], [6], [7], [8], [9]. In this framework, RF MEMS switches are micro-mechanical devices utilizing, preferably, a DC bias voltage for controlling the collapse of metalized beams [8]. Magnetic [10], thermal [11] and piezoelectric [12] actuations have been also evaluated, but the electrostatic one seems to be until now preferred for no current flowing, i.e. a virtual zero power consumption, less complicated manufacturing processes and more promising reliable devices [13]. During the last few years, several research activities started to release the feasibility of RF MEMS switches also for Space Applications [14], [15], [16]. The electrostatic actuation of clamped-clamped bridges or cantilevers determines the ON and OFF states depending on the chosen configuration. As well established, RF MEMS switches are widely investigated for providing low insertion loss [8], no or negligible distortion [17], [18] and somehow power handling capabilities [19], [20], [21], [22] for a huge number of structures already utilizing PIN diodes for high frequency signal processing. Actually, redundancy switches as well as single pole multiple throw (SPMT) configurations, [23], [24], matrices [25] true time delay lines (TTDL) [26], [27] and phase shifters [28], [29] for beam forming networks in antenna systems could benefit from their characteristics. On the

* Andrea Lucibello¹, Giorgio De Angelis¹, Emanuela Proietti¹, George Papaioannou², Giancarlo Bartolucci^{1,3}, Flavio Giacomozzi⁴ and Benno Margesin⁴

¹CNR-IMM Roma, Roma, Italy

²University of Athens, Athens, Greece

³University of Roma "Tor Vergata" – Electronic Eng. Dept., Roma, Italy

⁴Bruno Kessler Foundation, Center for Materials and Microsystems, Povo (TN), Italy

other hand, the reliability of this technology has been not yet fully assessed, because of the limitations introduced by: (i) the mechanical response of the single switches [30], (ii) the necessary optimization of the packaging [31], and (iii) the charging mechanisms. In particular, the charging effect is due to the presence of both the dielectric material used for the realization of lateral actuation pads, deposited to control the collapse of bridges and cantilevers far from the RF path, and the dielectric used for the capacitance in the case of shunt connected microstrip and coplanar configurations. Presently, there is a wide literature about the onset of the mechanism [32], [33], [34] and its control by means of uni-polar and bi-polar actuation voltage schemes [35], [36], [37]. Some results give evidence also for the substrate contribution to charging effects [39] and those related to packaging [38]. Specifically, electromagnetic radiation is a serious issue for space applications [40], [41]. Electrostatic discharge has been discussed in [42], and it is clearly influenced by the deposition process [43]. Besides structural dependence of the charging [44], solutions considering the absence of the dielectric material is also considered, giving evidence for a decrease but not for a complete disappearance for such a contribution [45], [46]. Specific aging schemes based on the temperature are also proposed for long term evaluation of the devices [47]. Advanced studies have been also performed by means of the Kelvin Probe Microscopy, for improving the surface resolution of the charging effect detection [48]. Ohmic contact problems have been evaluated in [49]. Different kind of charging mechanisms can influence the reliability of the MEMS devices, as it has been assessed after the study published in [50].

In this chapter, it will be presented the characterization of two configurations of RF MEMS switches, to demonstrate how the actuation voltage is modified by using a uni-polar bias voltage and how it is under control and stable, at least for a limited number of consecutive actuations, if an inversion in the bias voltage is provided. In particular, the measurements recorded for an ohmic series and for a shunt capacitive configuration will be presented and discussed, considering the main source of charging for both devices. Moreover, experiments performed in both MIM and MEMS reveal that the charging process is strongly affected by the temperature [51]. MIM capacitors have been used to assess the material bulk properties with the aid of Thermally Stimulated Depolarization Current (TSDC) method. The charge storage was found to increase exponentially with temperature in both MIM capacitors and MEMS switches. In particular, in the high temperature range the activation energies in MEMS switches were found to have close values with respect to MIMs, and from TSDC experiments in MIM capacitors they have been found to be rather small. Equivalent circuits accounting for the above charging effects can be used as an effective lumped model, useful for circuital simulations of feeding lines and actuation pads [52].

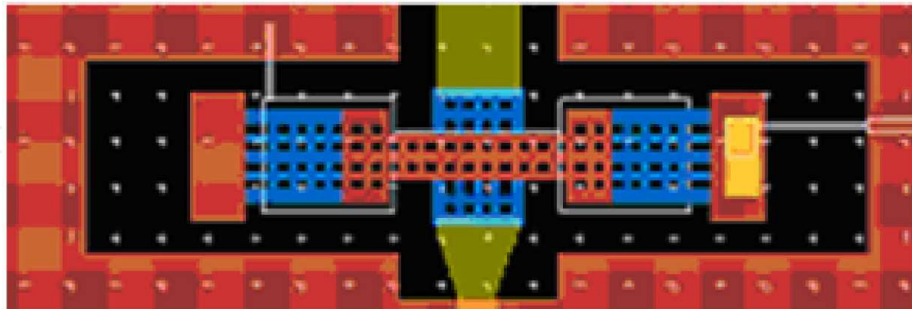
2. Technology

Suspended bridges have been manufactured in coplanar waveguide (CPW) configuration. The series ohmic switch has been obtained by means of a bridge isolated with respect to the lateral ground planes, closing a capacitive in-plane gap when the proper bias voltage is provided by means of lateral poly-silicon pads. In such a case the bridge is collapsed and the switch passes from the OFF to the ON state. *Vice versa*, the shunt capacitive switch is composed by a metal bridge connecting the lateral ground planes and by a dielectric layer providing a capacitive contribution when the bridge is collapsed. In this case, when the switch is actuated by means of a DC bias voltage, it passes from the ON state to the OFF

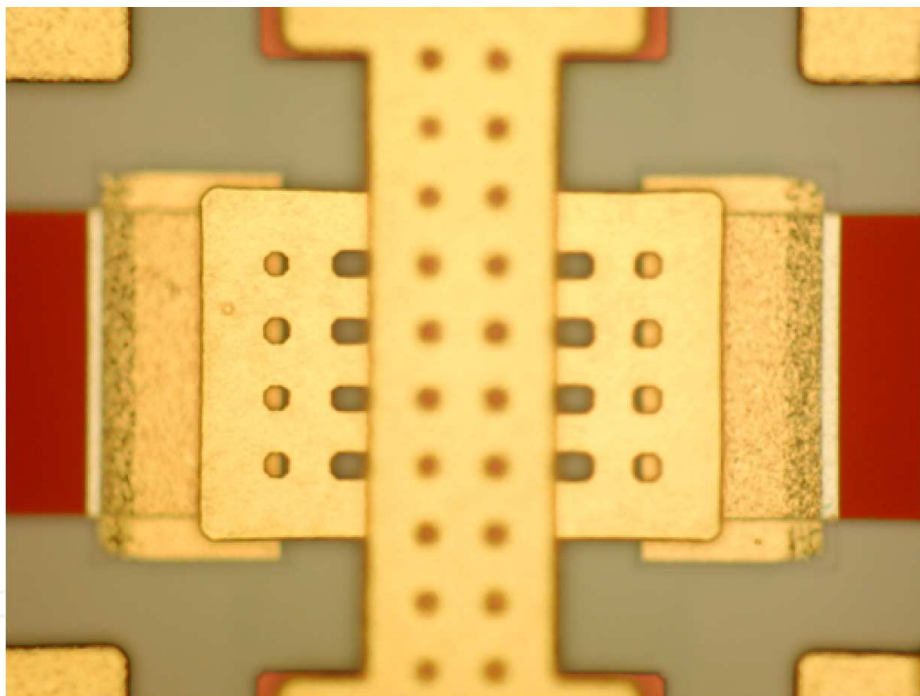
one. In order to fabricate micromechanical switches together with integrated resistors and DC blocking capacitors an eight mask process has been developed. Two electroplated gold layers of different thickness are provided for the realization of highly complex moveable bridges and the co-planar waveguides. The substrates are p-type, <100>, 525 μm thick, 5 $\text{k}\Omega\text{-cm}$ high resistivity silicon wafers. A 1000 nm thick thermal oxide is grown as an isolation layer. Next a 630 nm thick un-doped poly-silicon layer is deposited by low pressure chemical vapour deposition (LPCVD), to be used for the resistors and actuation electrodes obtained by selective dry etching of the poly-silicon layer. Then, tetra-ethyl-ortho-silicate (TEOS) is deposited by a LPCVD process to provide the high isolation needed for the actuation electrodes. Contact holes are then defined and etched by a plasma process. After ashing the photoresist mask, a multilayer underpass metal Ti/TiN/Al/TiN is deposited by sputtering. The total thickness of the multilayer has to be the same of the polysilicon, in such a way that metal underpass and actuation electrodes are at the same level. The wafer front side is then covered with 100 nm of low temperature oxide (LTO) to obtain an insulating layer for capacitive shunt switches. The previous step is un-necessary for series ohmic configurations. The vias in the LTO are defined by masking and dry etching. A Cr/Au layer is defined by lithography and wet etched. The main purpose of this layer is to cover with a noble metal the exposed electrical contacts of the series ohmic switches to get low resistive electrical contacts. The sacrificial layer required for obtaining the air gap is formed by a 3 μm thick photoresist, hard baked at 200 $^{\circ}\text{C}$ for 30 minutes to obtain well-rounded edges. As a seed-layer for electrochemical Au deposition a 10/150 nm thick Cr/Au layer is deposited by PVD. The moveable air bridges are defined using a 4 μm thick positive resist. After an exposure to oxygen plasma at 80 $^{\circ}\text{C}$ a 1.8 μm thick gold layer is selectively grown in a gold sulphite bath. The first plating mask is removed with an appropriate solvent and the CPW lines and anchor posts for the moveable air bridges are defined with 5 μm thick positive resist and then a 4 μm thick gold layer is selectively grown. The last plating mask and the seed layer are then wet removed. At this point a sintering in nitrogen at 190 $^{\circ}\text{C}$ for 30 minutes is performed to provide the gold layers with the appropriate tensile stress. Finally the air bridges of the individual switches are released with a modified plasma ashing process (20 minutes oxygen plasma at 200 $^{\circ}\text{C}$) in order to avoid sticking problems. The two devices which have been used for the characterization are shown in the photos given in Fig. 1 (series ohmic device, device S1) and in Figure 2 (shunt capacitive switch, device CL).

3. Experimental results

All the measurements have been performed and recorded in a Clean-Room environment, at the temperature $T=(23\pm1)$ $^{\circ}\text{C}$, with a relative humidity $\text{RH}=(35\pm1)$ %. A nitrogen flux has been used for providing a dry environment for the devices under test. RF measurements have been used as a validation for the state (ON or OFF) of the switches and for their electrical performances before, during and after the voltage application. In particular, after each cycle used for such a measurement, no changes in the electrical performances of the exploited devices has been recorded. A schematic diagram of the measurement bench is shown in Fig. 3. The reliability of the manufactured devices with respect to the charging effects, and specifically the influence of the pulse shape and of the sign of the voltage (positive or negative) on the actuation mechanism, have been studied by using pulse trains where the rise and fall time, as well as the pulse duration and the separation between pulses



(a)



(b)

Fig. 1. Diagram (a) and photo detail (b) of the implemented ohmic series switch configuration. Lateral wings have been included for improving the electrical contact. A number of switches with different geometrical and physical characteristics have been produced on the base of changes with respect to this one. Actually, the number of dimples as well as the thickness of the bridge and other details of the geometry contribute to the electrical performances. When the switch is actuated, the bridge, isolated with respect to the ground, closes the central conductor of the CPW with a metal-to-metal contact and the device is in the ON state (device S1).

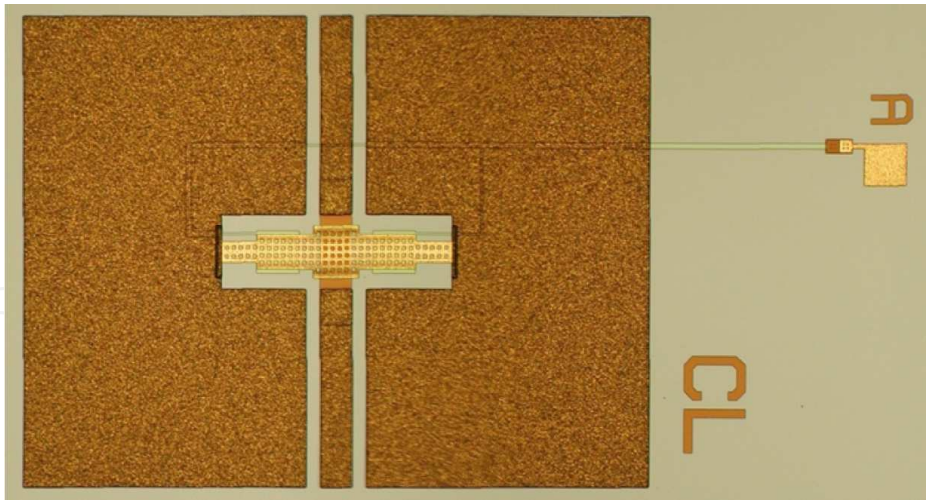
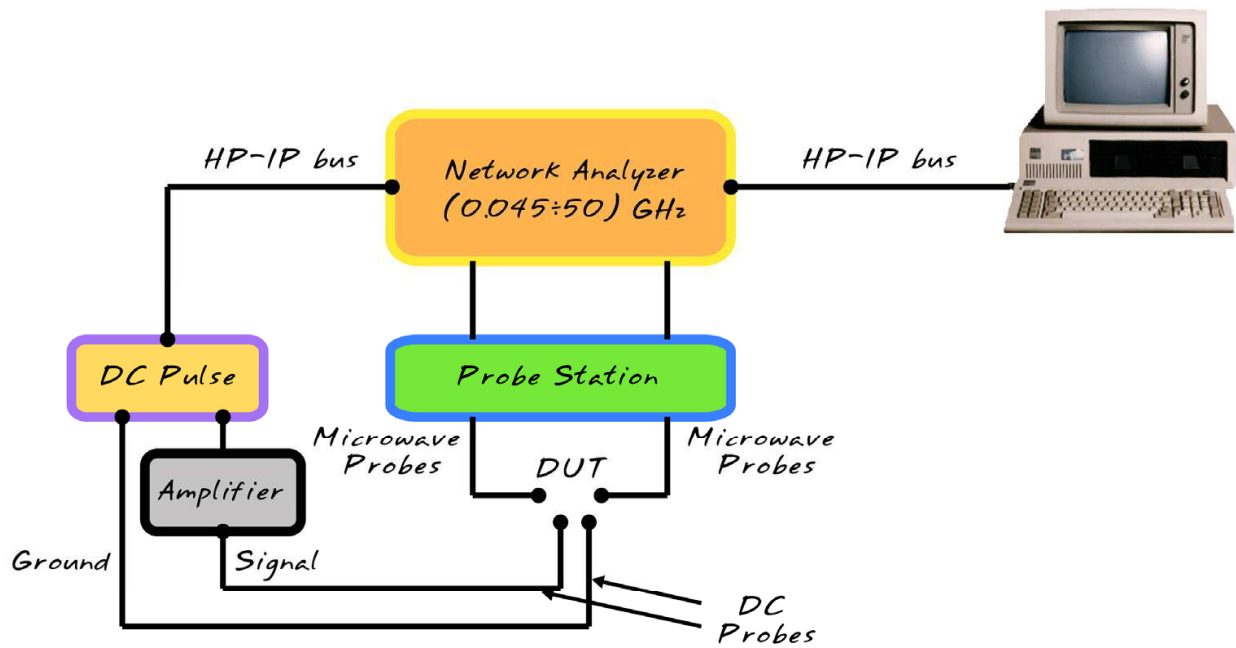


Fig. 2. Coplanar shunt capacitive switch. When the switch is actuated, the bottom side of the suspended bridge is collapsed, touching the dielectric layer placed along the central conductor of the CPW, providing a shunt to ground in a limited frequency range (resonant response), and the device is in the OFF state (device CL).



MEM-Switches : On-wafer characterization

Fig. 3. Schematic diagram of the measurement system used for testing the RF MEMS switches.

have been slowly changed. Moreover, a bi-polar scheme has been applied, with positive voltages followed by negative ones. For the uni-polar experiment as well as for the bi-polar one, the actuation voltage has been recorded when the sudden change in the measured Scattering Parameters due to the bridge collapse was clearly visible on the Vector Analyzer, i.e. by means of an abrupt change in the value of both transmission and return loss. Actually, this occurs during the voltage ramp.

In particular, we paid attention to:

- The pulse-width
- The rise-time and the fall-time of the pulses (ramps)
- The delay between the positive and the negative pulse
- The applied voltage

The first measurements have been performed by using only positive pulses (uni-polar scheme) with a ramp of 1 V/sec and $T_1=T_2=1$ min. After that, positive and negative pulses have been used, with the following parameters:

- Ramp=1 V/sec and 2 V/sec
- $T_1=1$ min and 30 sec
- $T_2=10$ sec.

Both devices given in Fig. 2 and in Fig. 3 have been characterized by using the proposed uni-polar and bi-polar schemes as it is explained in detail in the following text. In the uni-polar scheme, after the actuation, the switch is maintained at the same voltage during the time T_1 . Then, the voltage has been decreased down to zero, and in the meantime the de-actuation voltage has been measured. The successive ramp was imposed by increasing again the voltage until a new actuation occurs, and also in this case the voltage is maintained constant during the time T_1 . Every time, the voltage required for the successive actuation was higher than the previous one. The procedure was repeated for recording actuation and de-actuation voltages until a *plateau* value has been obtained. In the bi-polar scheme, the applied DC voltage is composed by positive and negative pulses having a maximum value of ± 50 V for the device in Fig. 1 (S1) and ± 60 V for the device in Fig. 2 (CL), and in this case the actuation and de-actuation voltages have been measured as absolute values of the imposed pulses. In Fig. 4 the shape of the pulse trains used in the experiments is shown.

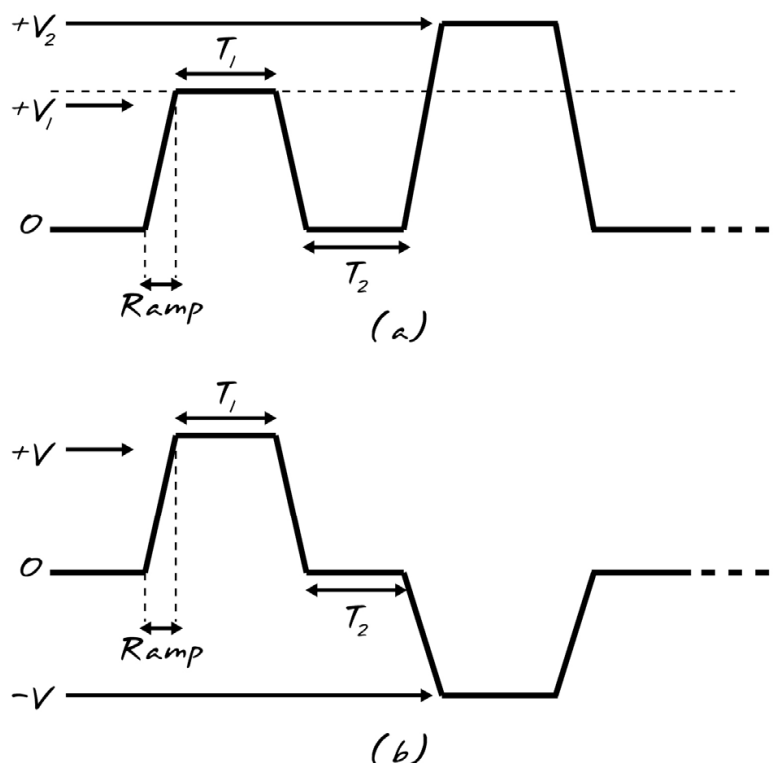


Fig. 4. Shape of the pulse trains used for the experiments on the charging effects. (a) is the uni-polar scheme, while (b) is the bi-polar one.

In the following text and figures, results and comments on the performed measurements are presented. First of all, S1 and CL have been actuated by using a uni-polar, positive voltage scheme. For both of them, the actuation as well as the de-actuation voltages have been measured until a *plateau* voltage has been obtained. The results are shown in Fig. 5 and in Fig. 6 with the values of the voltage and time parameters used for the actuation, and obtained for the corresponding de-actuation. In this case, the applied and measured voltages are always positive.

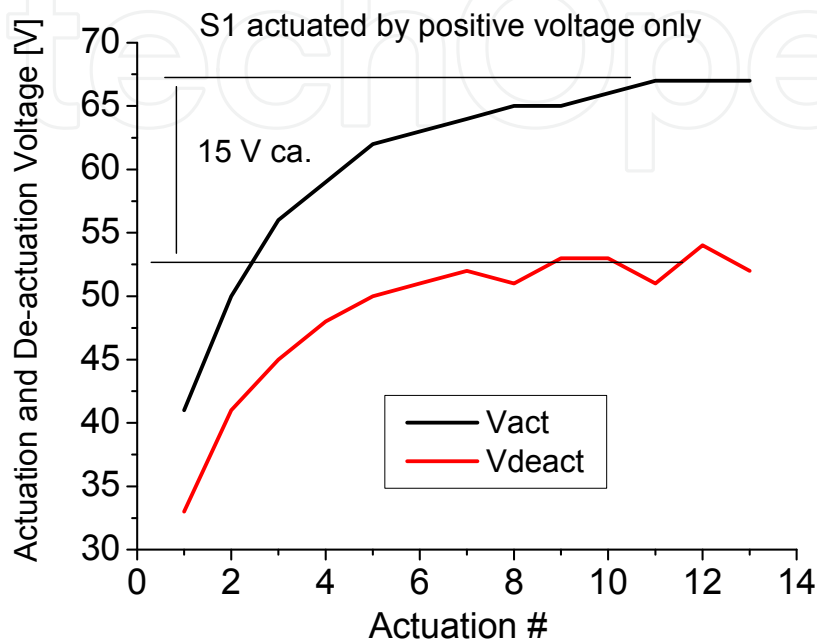


Fig. 5. Response of S1 actuated by using positive voltages only. T1=1 min, T2=10 sec, Ramp=1 V/sec for both trailing and leading edge of the pulse.

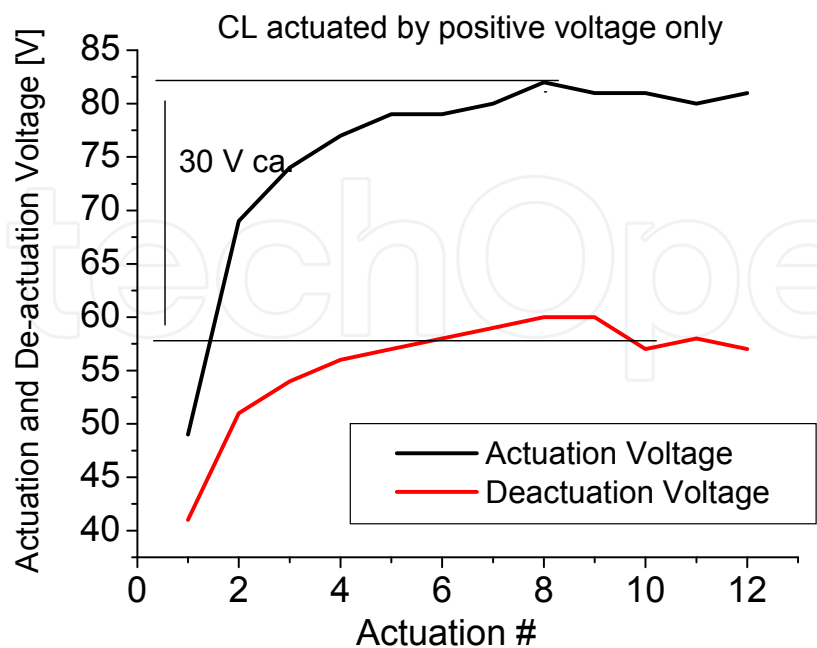


Fig. 6. CL actuated by using positive voltage only. T1=1 min, T2=10 sec, Ramp=1 V/sec, for both trailing and leading edge of the pulse.

Therefore, a bi-polar scheme has been applied by measuring the same devices the day after, when the effect of charging was completely removed, leaving them at rest without voltage nor RF signals applied to the device under test. The results are given in Fig. 7 and in Fig. 8, where the absolute value of the applied voltage is plotted as a function of the performed

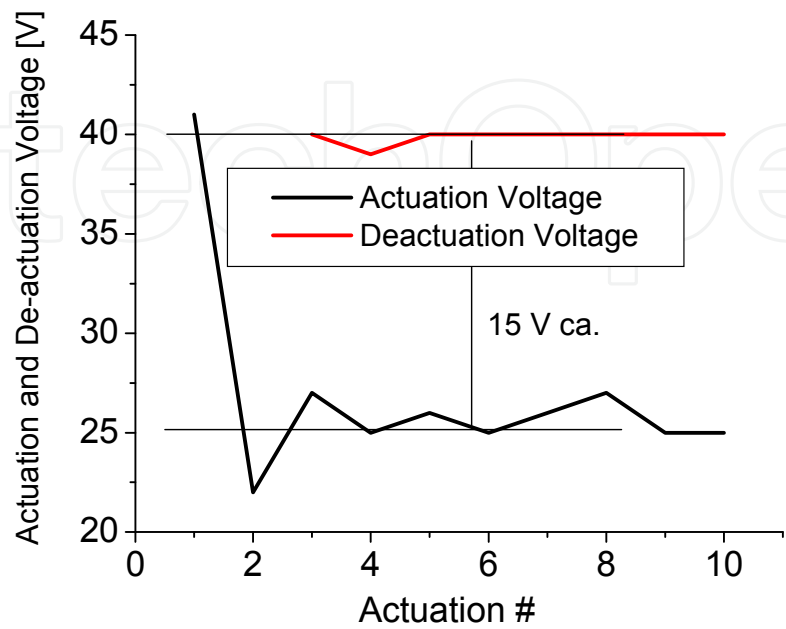


Fig. 7. S1 actuated by using positive and negative voltages. Only the absolute value of the recorded actuation voltage is plotted, but changed from +V to -V after each pulse, with $T1=1\text{ min}$, $T2=10\text{ sec}$, $|+V| = |-V| = 50\text{ volt}$ and $\text{Ramp}=1\text{ V/sec}$.

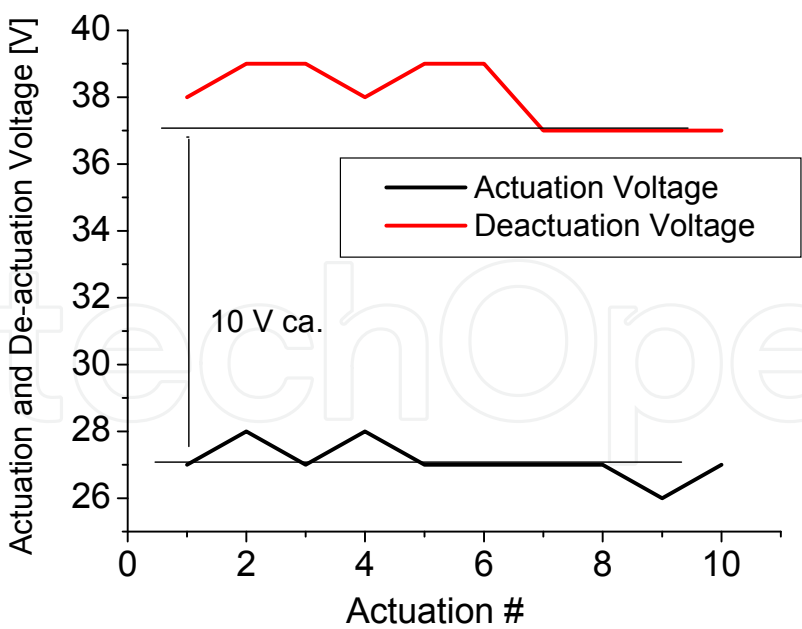


Fig. 8. S1 actuated by using positive and negative voltages. Only the absolute value of the voltage is plotted, but changed from +V to -V after each pulse, with $T1=30\text{sec}$, $T2=10\text{ sec}$, $|+V| = |-V| = 50\text{ volt}$ and $\text{Ramp}=1\text{ V/sec}$. The measurement has been performed 5 min after the one shown in Figure 7. The difference between actuation and de-actuation voltages is a bit decreased, which is an indication of a charging partially re-covered.

actuations. It is worth noting that the measured data have been normalized to positive values, and the reader can have the erroneous feeling that the de-actuation voltage is always higher than the actuation one. This is only a false perspective, and the reason for such a finding is discussed after the presentation of the experimental data.

It is worth noting the difference obtained between the results in Fig. 7, Fig. 8 and Fig. 9. Actually, no dependence on the applied ramps has been obtained, but there is a clear evidence that the process is quite slow, because after times in the order of several minutes, i.e. during the experimental procedure, the charging is still present. From the analysis of the figures where both positive and negative voltages have been applied (Fig. 7, 8 and 9), one could conclude that the actuation voltage is lower than the de-actuation one. In fact, this is due to the kind of plot, because only the absolute value of the applied voltage is given, in order to have a continuous curve, with data not jumping from negative to positive values. The physical reason for that is explained in the discussion at the end of this section.

In the following Fig. 10 and Fig. 11 the same qualitative results are shown for the device CL, where in 30 minutes ca. the charging effect has been almost completely recovered. It turns out from this finding that the same values for the actuation voltages have been recorded, and the same difference between $V(\text{actuation})$ and $V(\text{de-actuation})$ has been obtained.

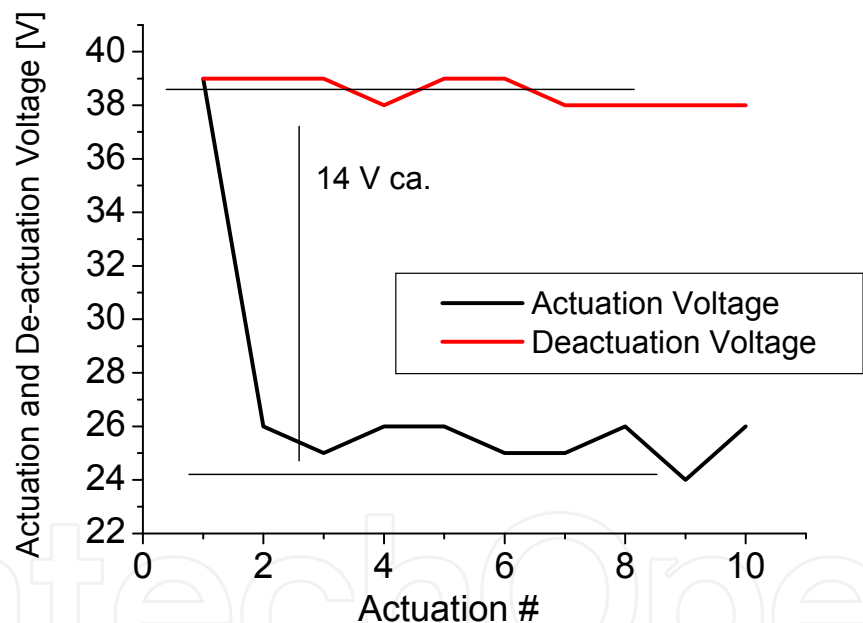


Fig. 9. S1 actuated by using positive and negative voltages. The same parameters used in the previous Fig. 8 have been imposed, i.e.: $T_1=30$ sec, $T_2=10$ sec, $|+V| = |-V| = 50$ volt and Ramp=2 V/sec. The measurement has been performed the day after. The result is quite similar to that shown in Fig. 3, with T_1 decreased from 1 min to 30 sec and Ramp passed from 1 V/sec to 2 V/sec. As a consequence, none of the above parameters seems to affect the measures. Moreover, the first actuation is still between 39 and 41 V, but by using positive and negative values it is maintained at a constant value as well as the de-actuation voltage, and it is lower than in the positive case only.

Some of the main findings of the performed measurements are in full agreement with those in [34], and in particular with the conclusion that the devices do not fail if they are subjected to a square wave voltage for the actuation when a C/V curve is taken with a slowly varying

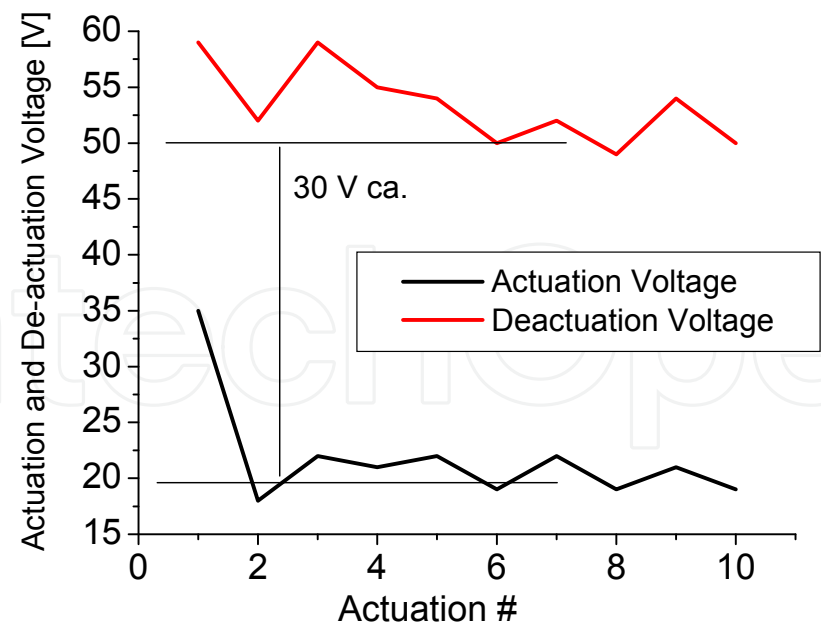


Fig. 10. CL actuated by using positive and negative voltages. $T_1=1$ min, $T_2=10$ sec, $|+V| = |-V| = 60$ V and Ramp=1 V/sec.

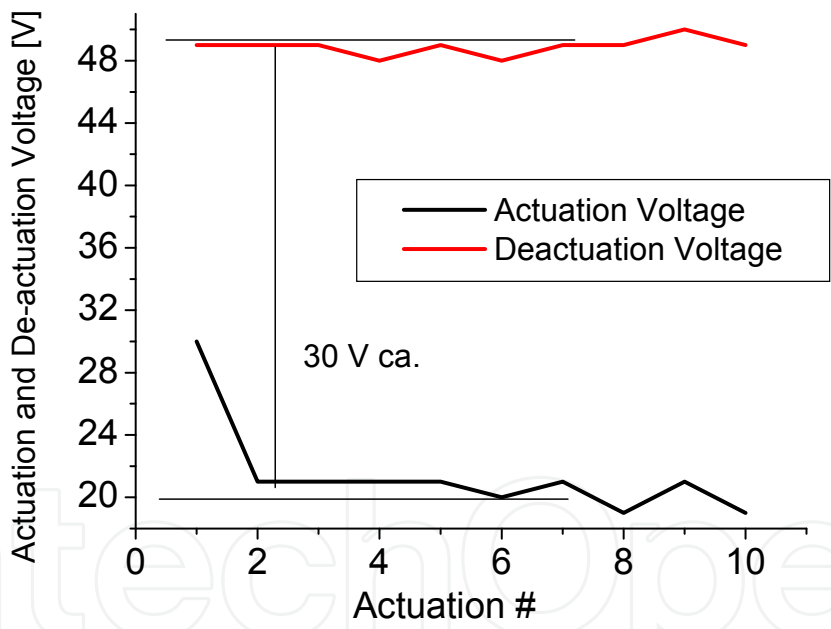


Fig. 11. CL response by using the same parameters as in the case of Fig. 10, but with Ramp=2 V/sec and measurement performed after 30 min. The difference between the two levels has the same value as before.

voltage. Actually, for slow ramps we never experienced a stuck device for both S1 and CL. On the other hand, the reliability tests previously performed on the same devices were never accompanied by a sticking of the series configuration, in spite of the fact that a faster switching was used in that case [47]. It is clear, in the present experimental results, that charging effects are present in both configurations, affecting in a predictable way the performances of the measured devices. In particular:

- The absolute value of the actuation voltage V_a and of the de-actuation voltage V_d (and the difference between them) is constant when the sign of the pulse is reversed, exception done for the first actuation
- The measured difference in the bi-polar scheme is equal to the difference between the two plateau (i.e. $V_{a,plateau} - V_{d,plateau}$) experienced during the charging process when a positive voltage pulse train is applied. This could be used as a measure of the maximum charge which can be accumulated in the device
- The absolute value of the actuation voltage for the series switch S1 is almost half of the first positive value when a train of positive and negative pulses is used
- The absolute value of the actuation voltage for the shunt switch CL subjected to positive and negative pulses is around 20 volt Vs the almost 55 volt used for the positive voltage only.
- The results from the previous two points are “re-normalized” considering that the algebraic sum of the positive actuation voltage (starting from the second actuation), and of the difference between the two plateau values in the case of positive only voltages ($V_{a,plateau} - V_{d,plateau}$), gives as a result the first positive actuation voltage. This means that the voltage difference necessary for the actuation is the same. So, when positive and negative voltages are applied to the device S1, for which we have $|V_a| \approx 40$ V, then, after the first de-actuation (occurring in this case again at $V=40$ V after imposing $V=50$ V) we always get $|V_a| \approx 25$ V with a difference of 15 V coming from the extra voltage generated by the charging effect due to the previous actuation.
- The same result is obtained for the CL configuration, where $|V_a| \approx 50$ V, and the first de-actuation occurs at $|V_d| \approx 50$ V after imposing a positive voltage $V=60$ V. After that, the switch is actuated always by applying 20 V. Actually, a difference of 30 V is always observed (in this case this happens independently of the time passed from the previous measurement), in such a way that the sum $20+30=50$ V is again the value of the first actuation voltage experienced when positive only pulses are used.

As a consequence of the above discussion, both schemes for actuation (uni-polar and bi-polar) are affected by charging mechanisms, because the dielectric is always present. On the other hand, the bi-polar scheme offers the advantage, with respect to the uni-polar one, in terms of the absolute value of the voltage necessary for actuating the device [37]. This is especially good when a high number of actuations are needed for a frequent re-configuration of architectures based on several RF MEMS, and there is no time for a full de-charging of each individual device. In our devices, we believe that the charging exhibits a saturation value due to the maximum number of charges which can be activated on the surface as well as in the bulk of the dielectric, which slowly goes back to the original situation. In this framework, looking at our experimental results, the utilization of positive and negative pulses allows a faster re-combination process, and the possibility to drive the device always by means of the same absolute value of the voltage, changing the sign of the applied voltage from one actuation to the successive one. A possible interpretation could be that the de-charging process, usually slow, is accelerated when the device is subjected to a gradient of the electric field, passing from positive to negative values and vice-versa. In the following Fig. 12 the bi-polar scheme imposed for S1 and the effect on the actuation voltage is shown.

4. Measurements on test MIM capacitors and discussion

MIM capacitors having the same structure to be used for the actuation pads of the RF MEMS switches have been realized, to study the charging mechanisms related to the materials used

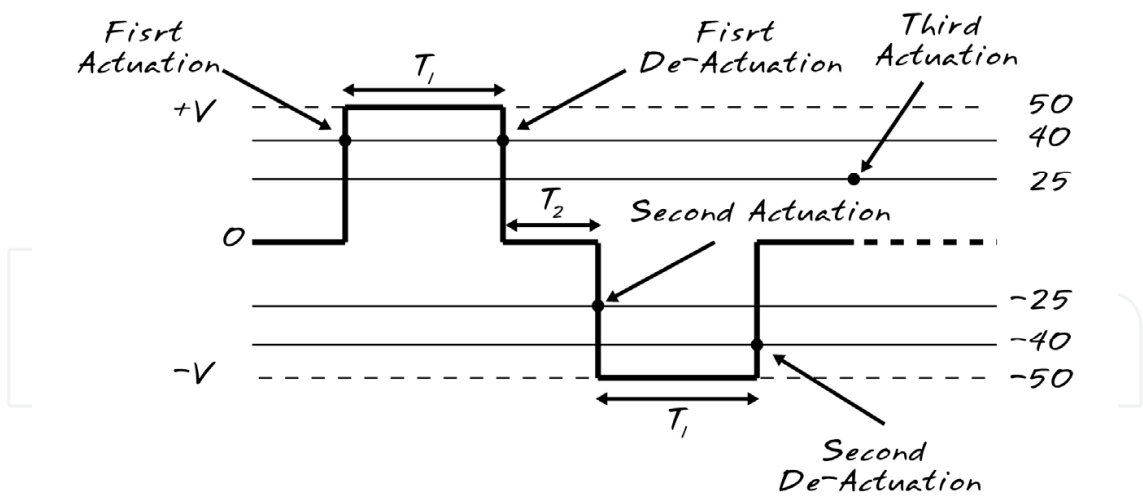


Fig. 12. Bi-polar scheme imposed for the actuation of the switch S1.

for the device actuation. It is worth noting that the MIM is only an approximation of the real actuation, because in this case no residual air gap has to be considered between dielectric and metal bridge. For this reason the MIM should suffer for charging and de-charging effects different with respect to those measured on the real device for both time and kind of processes. On the other hand, it is important to know the properties of the material itself, because it will affect the operation of the device. The scheme and related equivalent circuit of the measurement setup used for characterizing the MIM is shown in Fig. 13. In Fig. 14 the two structures used for the MIM devices are also shown.

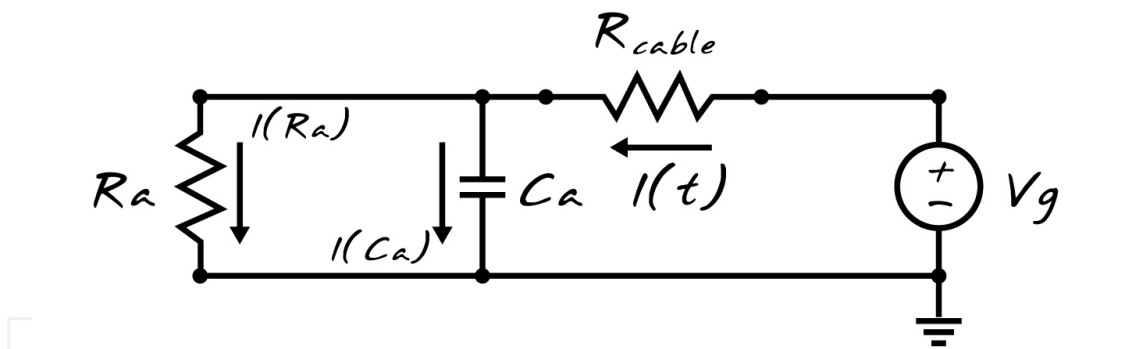


Fig. 13. Equivalent circuit for the measurement setup of the MIM Capacitors. A power supply provides the voltage V_g and the current I , both functions of the time t following a slow ramp. The device under test is a MIM simulating the actuation pad structure, schematized as a capacitor C_a with a high bulk resistance R_a in parallel with respect to C_a .

From the analysis of Fig. 13, the equations governing the voltages and currents on the equivalent lumped components can be written as:

$$\begin{aligned} I(t) &= I_{Ca}(t) + I_{Ra}(t) = C_a \frac{dV_{Ca}(t)}{dt} + \frac{V_{Ca}(t)}{R_a} = \frac{-V_{Ca}(t) + V_g(t)}{R_{cable}} \\ V_{Ca}(t) &= V_g(t) - R_{cable} I(t) \\ \frac{dV_{Ca}(t)}{dt} &= \frac{dV_g(t)}{dt} - R_{cable} \frac{dI(t)}{dt} \end{aligned} \tag{1}$$

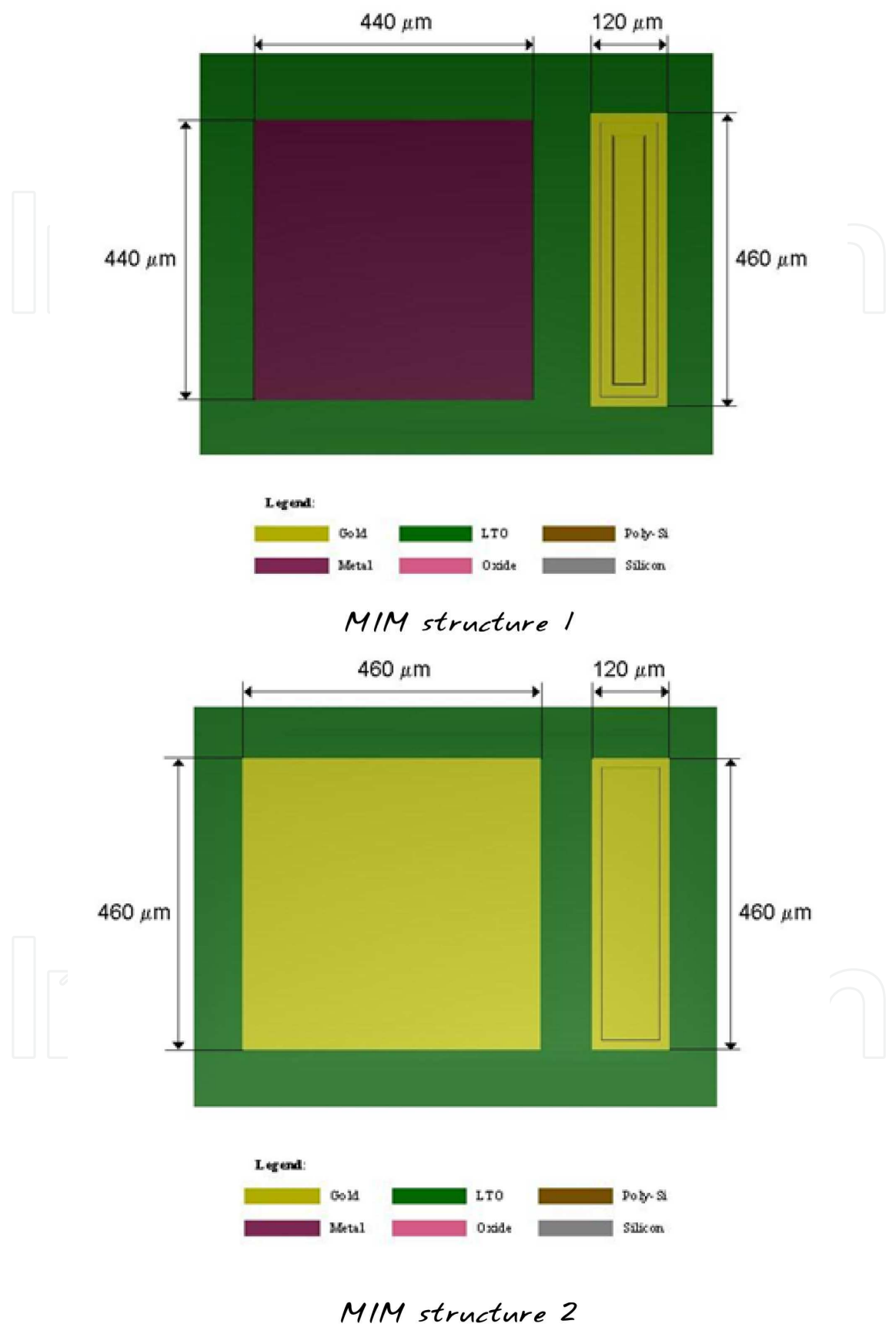


Fig. 14. MIM structures used for the characterization.

From the above equations, it turns out that the measured value of $I(t)$ when imposing $V_g(t)$ will be given by using the following relation:

$$\left(1 + \frac{R_{cable}}{R_a}\right) I(t) = C_a \frac{dV_g(t)}{dt} + \frac{1}{R_a} V_g(t) - C_a R_{cable} \frac{dI(t)}{dt} \approx I(t) \quad (2)$$

The last assumption is valid when, as it can be reasonably assumed, $R_{cable} \ll R_a$.

From the analysis of the measurements, it will be evident that when the dielectric material of the MIM behaves as an almost ideal dielectric, only the first term on the right hand of the above equation is important, and mainly a capacitive contribution is measured, as expected. Actually, the imposed ramp and the measured current will vary maintaining a constant ratio. On the other hand, because of the non-ideal response of the obtained dielectric material, a parallel resistance has to be included, to account, since the very beginning, for some free charges, and for the asymmetry in the capacitor itself, which has two parallel plates not equal between them for both dimensions and conductivity. So far, a capacitive response is obtained, strictly speaking, only at low voltage levels, and a small charge injection is immediately recorded, evidenced by a linear contribution typical of the second term in Eq. (2). An almost negligible contribution is also given by the last term of the same equation, being the derivative of the current very small and the resistance of the cable small too. The Poole-Frenkel effect, which should dominate the charging processes in the exploited dielectrics, begins to be evident when sufficiently high voltages are imposed after the first ramp, i.e. when V_g is in the order of tens of volt, and the recorded current suddenly increases. In this range, the response of the measured current follows a high-voltage law, while it is almost linear for lower values of V_g .

After some critical value of V_g , the picture given by Eq. (2) has to be strongly modified accounting for the change of both the conductivity and the polarization, which should influence at least the value of R_a .

In particular, the term describing the current flowing in R_a should be better identified by the formula suggested in [61] and [63] for high voltages. Moreover, we can map the time variable t into the applied voltage V_g , as the measurements are performed by using an I Vs V_g plot and, since the voltage is imposed by means of a linear ramp, we can also define $r = dV_g/dt = \text{const.}$

In the region of non-linear response for the current Vs voltage, the trend looks like coherent with conclusions in [61], where a dependence on V_g^2 is expected, following also the conclusions in [63]. This will transform Eq. (2) in:

$$I(V_g) = C_a \frac{dV_g}{dt} + f(V_g) - C_a R_{cable} \frac{dI}{dV_g} \frac{dV_g}{dt} = C_a \left(1 - R_{cable} \frac{dI}{dV_g}\right) r + f(V_g) \quad (3)$$

Which is valid until the breakdown occurs in the MIM structure, and $f(V_g)$ is a function involving the applied voltage, which is linear like in Eq. (2) until a high voltage dependence is required, as mentioned in [61] and [63]. Because of the charging effect and of the current induced by the Poole-Frenkel effect, Eq. (3) has to be corrected again when a second ramp is applied before the dielectric is naturally de-charged, and the effect will be a current decrease at the same voltage level experienced during the previous ramp. In this case, the Poole-Frenkel current (linked to the current density by $I_{PF}(V_g) = A J_{PF}(V_g)$) has to be included, having a sign which is opposite with respect to $I(V_g)$.

Wafer #	Dielectric	Thick. [nm] \pm 2%	Sample #	V_B [volt]	Charge Injection
1 BE: P TE: Al 1%Si	Nitride	98	C2	> 100	Few volt
			C3	> 100	Few volt
			C3	> 100	Few volt
			C4	> 100	Few volt
			C5	> 100	Few volt
3 BE: P TE: Al 1%Si	TEOS	203	C1	> 100	Few volt
			C2	> 100	Few volt
			C5	> 100	Few volt
4 BE: P TE: Al 1%Si	LTO	114	C6	\approx 100	Few volt
5 BE: P TE: Al 1%Si	PECVD Nitride HF	100	C2	\approx 75	Few volt
7 BE: Al 1%Si+ Ti+TiN TE: Cr / Au	LTO	114	C6	\approx 62	10-20 volt
9 BE: Al 1%Si+ Ti+TiN TE: Cr / Au	PECVD Oxide LF Top	78	C2	\approx 47	?
			C3	< 40	?
			C5	< 40	?
10 BE: Al 1%Si+ Ti+TiN TE: Cr / Au	PECVD Nitride HF	100	C1	?	> 10 volt
			C6	45	> 10 volt
11 BE: Al 1%Si+ Ti+TiN TE: Cr / Au	PECVD Nitride LF	87	C6	35	> 10 volt

Table 1. Full list of the measured devices. The wafer #, with the bottom electrode (BE) and the top electrode (TE) are given, with the dielectric and deposition technique. P is for Poly-silicon. The thickness is in nm \pm 2%. The breakdown voltage V_B is also shown, when it was possible to measure it. Charge injection is almost immediately recorded in many cases. HF and LF stand for high frequency and low frequency of deposition respectively.

Several wafers have been characterized, with repeated structures like those shown in Fig. 14. Actually, TEOS, LTO and Nitride (Si_3N_4) deposited following different methods have been obtained. Top and bottom electrodes have been changed too. The material and structural parameters are summarized in the following Table 1. Ramps of 0.05 and 0.1 V/s have been imposed. In particular, Wafer from #1 to #5 emulate the structure of the actuation pads, while from wafer #7 to #11 the situation of the underpass in the area of the bridge is proposed. A selection of the measurements performed on the samples is given in the following figures. The findings in Fig. 16 have been interpreted as the contribution of the electric field generated by: (i) trapped charges, and (ii) interface states. Both effects contribute in the opposite way

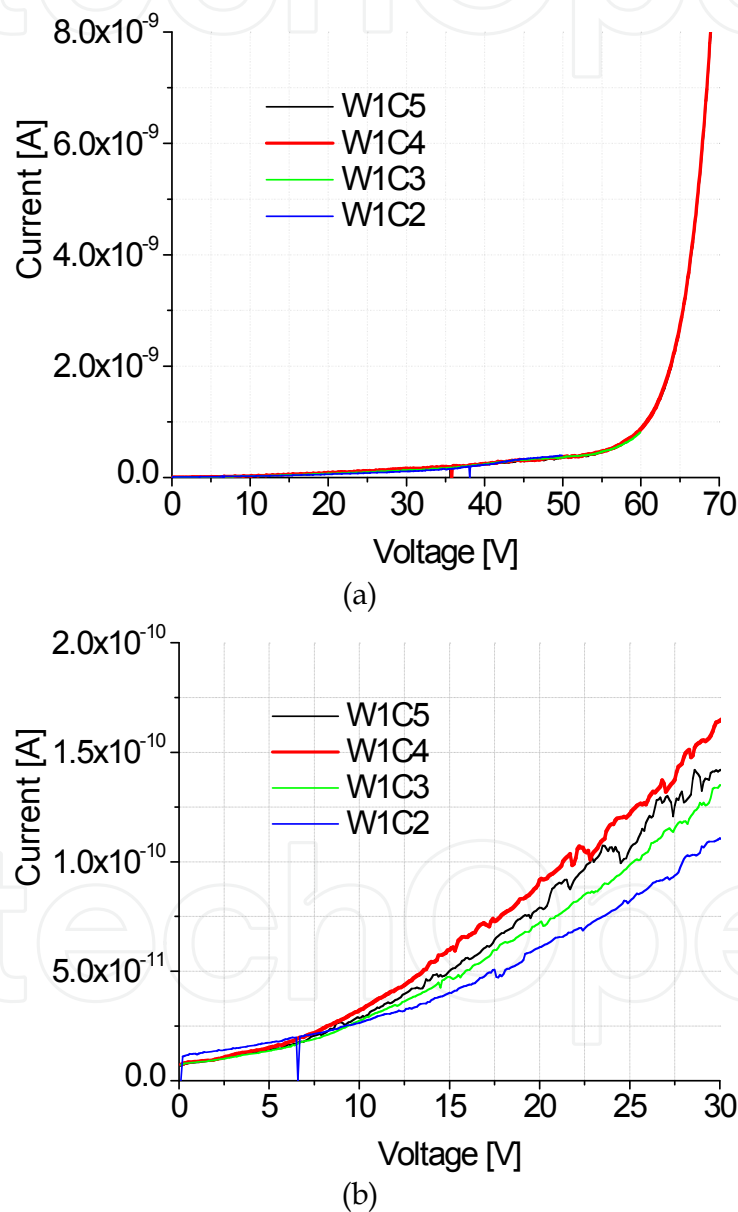


Fig. 15. I vs V for wafer #1 (W1). The same response (a) is obtained for different samples (C2, C3, C4, C5) having the same geometry and dielectric (nitride, Si_3N_4). Small differences can be seen only at low voltage and current values in (b) and can be attributed to the technological reliability. Actually, a charge injection is anyhow measurable, as the current response is not flat as a function of the applied voltage.

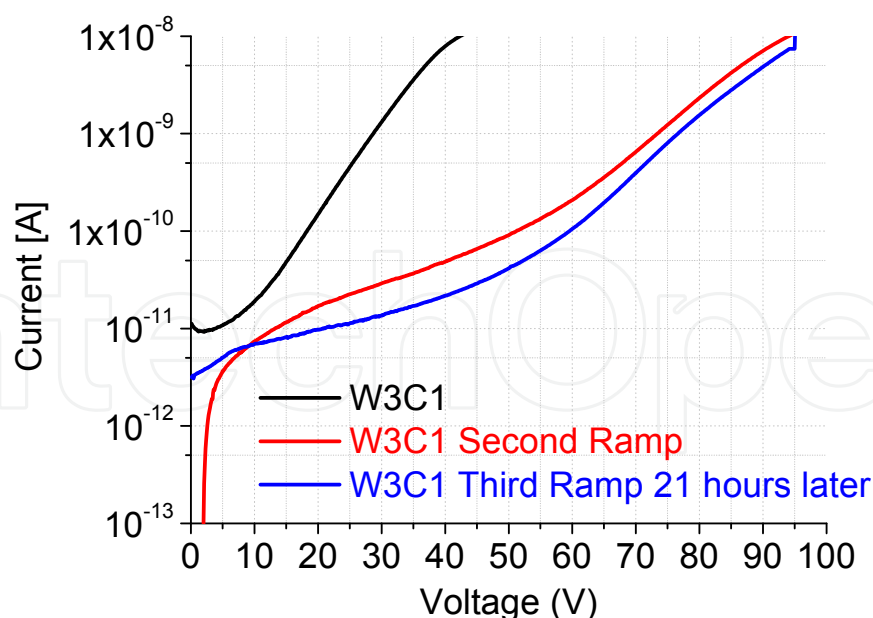


Fig. 16. I vs V for sample C1 in wafer #3 (W3C1, TEOS). A second ramp has been imposed after one minute, with clear evidence for the sample charging. The same behavior is exhibited by the other TEOS devices. The measurement has been repeated almost one day after the first one (21 hours later). In this case, the initial conditions are not yet restored, as it has been measured in other samples too.

with respect to the external DC field due to the actuation voltage. As a result, the sample experiences a decrease in the current flowing through the device. More in detail, the response of the dielectric is characterized, when the second ramp is applied, by a negative current for a relatively long time (40 sec ca. for a bias sweep rate of 50 mV/sec). This finding can be explained in terms of the additional contribution of the interface states, providing an increase in the number of charges. Actually, the trapping mechanism does not allow the injection of further charges, whereas the interface states can provide such an additional current, always opposite with respect to that induced by the external DC bias. This behavior has not been experienced 21 hours after because this long time allows the natural discharging process of the interface states. On the other hand, in almost one day, the trapped bulk charges had not the time for a full restoring of the initial conditions. In fact, during the third ramp a further positive shift of the voltage necessary for the onset of the charging process has been measured, in spite of the long time passed between the second and the third ramp.

The contribution of the electric field generated by the trapped charges and by the interface states is also evidenced in the plot of Fig. 17 for wafer #1, but a bi-polar actuation scheme has been adopted, instead of the uni-polar one used for the previous measurement. The results in Fig. 17 have been interpreted as it follows: from 0 to 80 V, during the first ramp, the dielectric is charged. From 80 V to 0 it is like to impose a second ramp (negative or positive slope it does not matter) and the current is down-shifted. In the third ramp it looks like to have the dielectric fully de-charged because of the second ramp, as the current response is symmetric with respect to the first ramp. During the fourth ramp, the current is increased in absolute value, with a peak probably due to a “frozen” charge. After that, the fifth ramp gives a response qualitatively similar to the previous plot, but higher values are recorded because the residual current is in the same sense with respect to the imposed one. It is worth noting that the measurements have been re-normalized to the first quadrant, as negative currents correspond to negative voltages. The findings in Fig. 17 have been

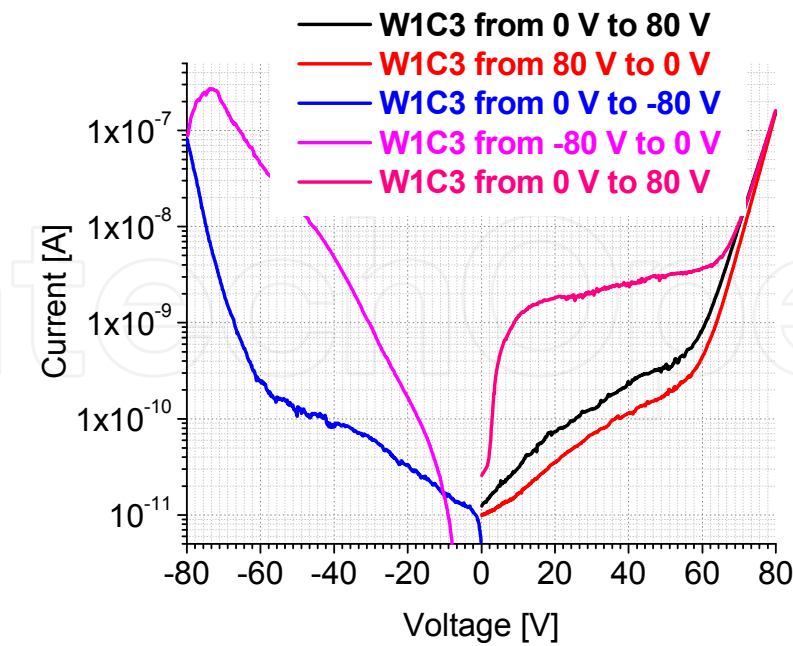


Fig. 17. The sample C3 from wafer #1 (W1C3, Si₃N₄) has been subjected to voltage ramps going forth and back up to a maximum value of ±80 V. As a result, a down shift of the current response is obtained by applying a voltage from 0 to 80 V and back from 80 V to 0. Then, an almost symmetric response is obtained when a negative bias is imposed. A completely different trend is measured by decreasing the applied voltage to 0, and finally a current increase is experienced going again to 80 V. Similar responses have been obtained for other samples.

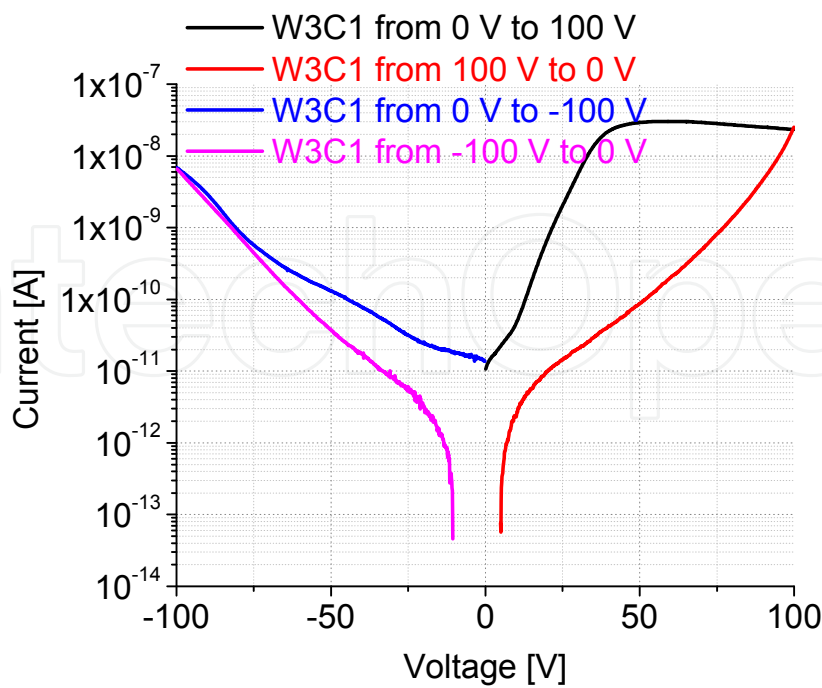


Fig. 18. The sample C1 of wafer #3 (TEOS) was measured by imposing a full cycle from positive to negative values and back to zero as it was in the data of Fig. 17.

interpreted again as the contribution of the electric field generated by the trapped charges and by the interface states, but in this case the field is in the same way with respect to the external one. Moreover, LPCVD Si₃N₄ shows a better response in terms of charge injection, because it happens at higher voltage values with respect to SiO₂. When the second ramp is imposed (Fig. 17) the absolute value of the current is higher with respect to the first one. At this stage, a de-charging effect is experienced, and the new charging process is evidenced at about 60 V, like in the first ramp, when it occurred at -60 V. It means that when a bi-polar scheme for the actuation is imposed, a fast de-charging is experienced, similarly to what occurs in the case of RF MEMS switches. In Fig. 18, the results for a TEOS based MIM in wafer #3 are shown. Looking at Fig. 18, a peak similar to the application of a negative bias experienced by the Si₃N₄ in the previous measurements (but less pronounced) is recorded also for TEOS during

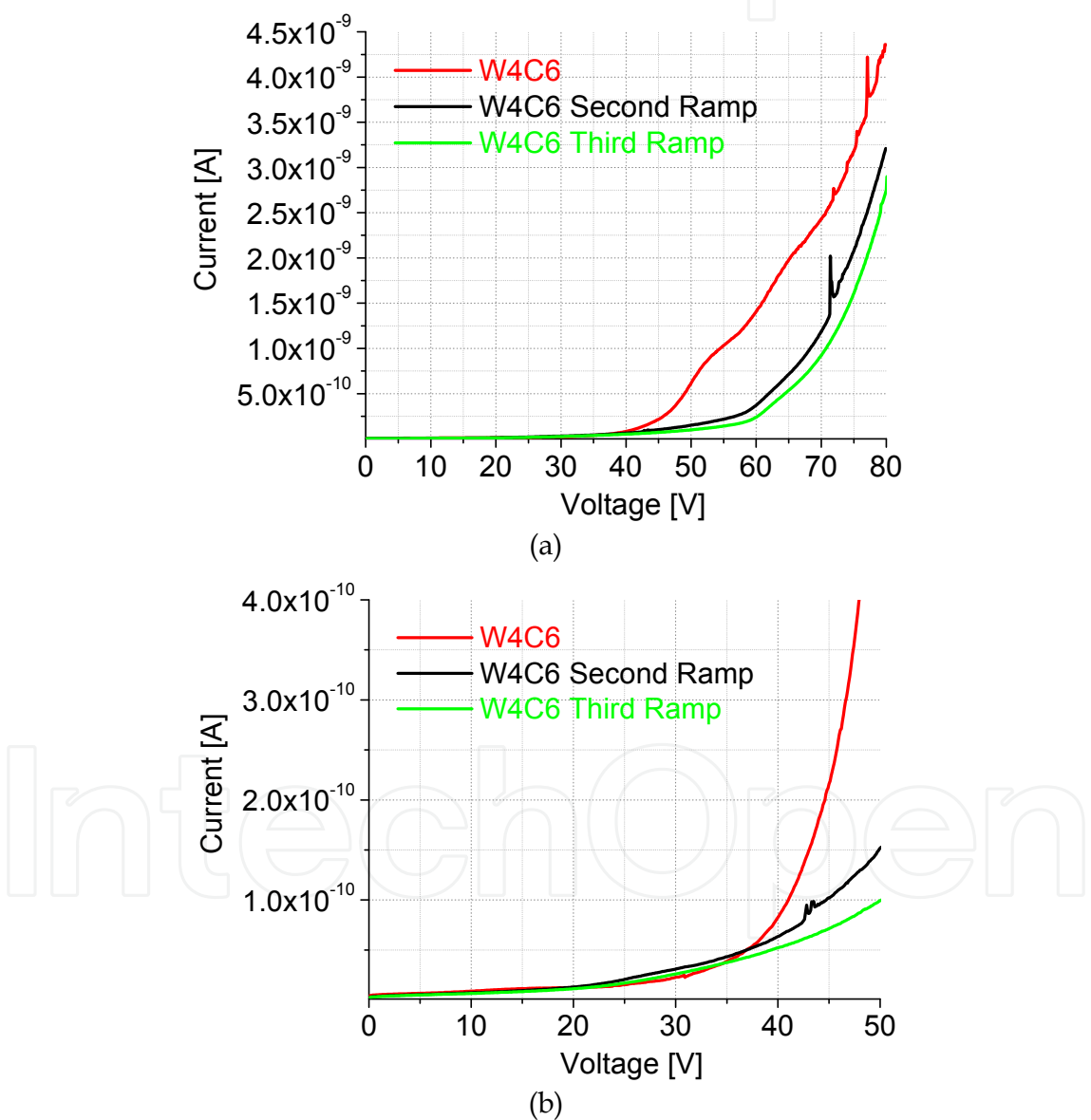


Fig. 19. The sample C6 of wafer #4 (W4C6, LTO) was measured by repeating the ramp three times (a). The charging process is enhanced, but the effect is less important the third time, thus suggesting the possibility for a saturation of the charge injected in the sample, which is not visible in (b), being the voltage below the threshold for the onset of the charging effect.

the first ramp (0 - 100 V), probably due to the same proposed effect of “charge freezing” for the previous material. A negative current is obtained by means of the second ramp (100 - 0 V), increasing the absolute value. When V_g is low and the capacitor is almost de-charged, current is injected in the opposite way, changing the slope with respect to the first ramp. During the fourth ramp (-100 - 0 V) the sample is de-charged again and the charge is newly injected at low voltage values. Ramps have been imposed again on an LTO based MIM from wafer #4, and plots in Fig. 19 and 20 give evidence for charging mechanisms when always the positive voltage is applied in successive ramps. As expected, the charging process is enhanced, but the effect is less important the third time, thus suggesting the possibility for a saturation of the charge injected in the sample.

For the wafer #5 and #7 the measured current increases with respect to the first ramp, as it is shown from Fig. 20 to Fig. 22.

In the case of PECVD Oxide LF Top in wafer #9 the response is the same recorded for wafers from #1 to #5. As a further characterization, one sample was subjected to DC cycling in a way analogous to that used for real RF MEMS switches. Specifically, the sample C2 belonging to Wafer #1, was measured after imposing a uni-polar train of 10^4 pulses with amplitude $V_g=50$ V, having a pulse-width $\tau=250$ ms and a period $T=500$ ms. Since the data obtained on this wafer are superimposed for all the measured samples, we used one C3 device, exactly equal to C2, as a reference structure. The result was an almost ideal dielectric response for low voltage values, i.e. a constant value for the current as a function of the applied voltage. The C3 structure, which was not “stressed” in the same way, behaves exactly as it was in the previous measurements, with a linear response of the current as a function of the voltage, starting from the very beginning. We believe that the above treatment was useful for helping the recombination of charges left free from the technological processes at the interface metal-dielectric, which were sensitive to the voltage gradient experienced during the application of the train of pulses, and especially to the sudden gradient imposed in correspondence of the trailing and leading edge of the pulses. The result is presented in Fig. 23.

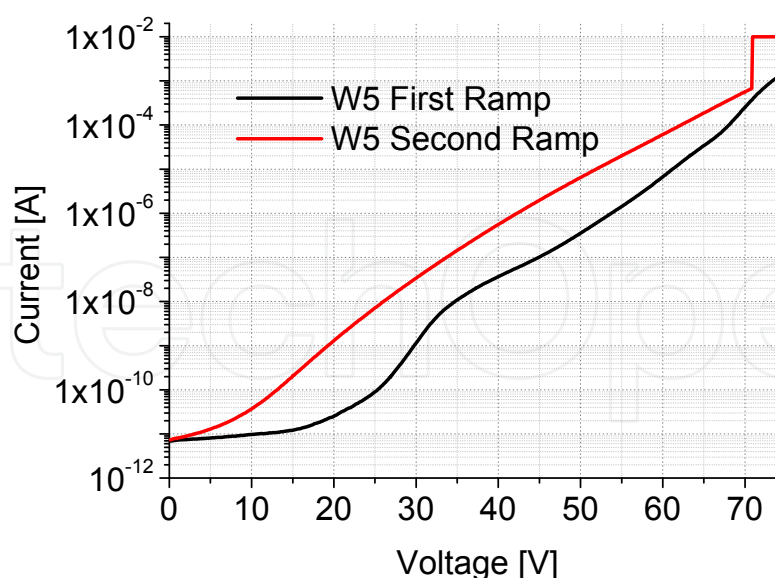


Fig. 20. Wafer #5 (PECVD Nitride HF). Shift of the current by using the same ramp and maximum value of the applied voltage, V_{max} , in two successive measurements separated by one minute ca. After the first ramp the nature of the dielectric was dramatically changed, thus exhibiting an up-shift of the measured current. The second time we are almost at the breakdown voltage, around 70 V.

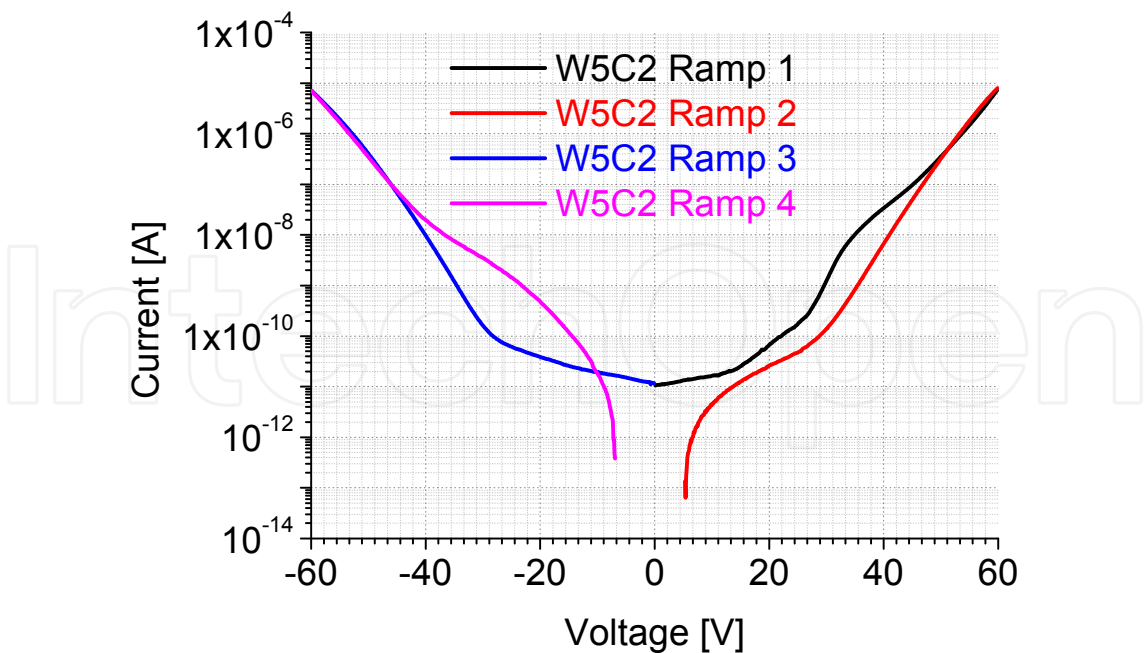


Fig. 21. I vs V for wafer #5, sample 2 (W5C2, PECVD Nitride HF). It is worth noting that there is not serious current reversal as it happened to TEOS. Actually, the difference with respect to the results for TEOS could be due to a higher densification temperature during the film preparation, reducing the contribution of free charges.

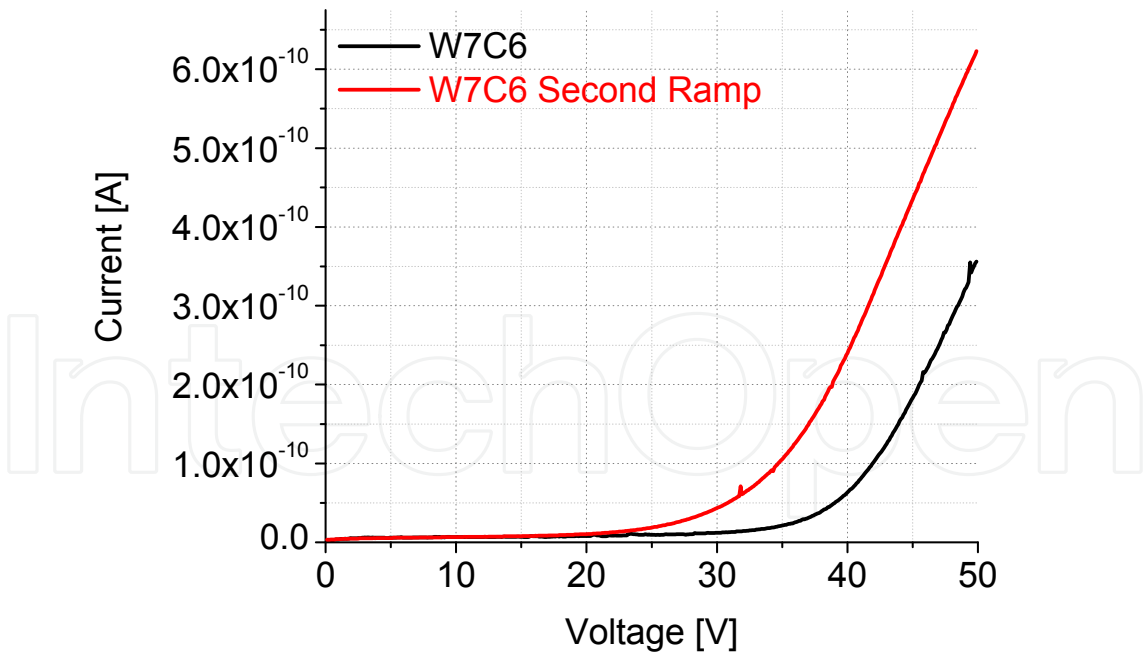


Fig. 22. I vs V for sample C6 in wafer #7 (W7C6, LTO). In this case the same structure present in the centre of the bridge is realized, with a multilayer as a bottom electrode and gold as the top one. Actually, an up-shift of the current is measured. As in the case of wafer #5 in Fig. 20, we were very close to the breakdown, around 62 volt, and this could change the general characteristics of the sample when the second ramp is used.

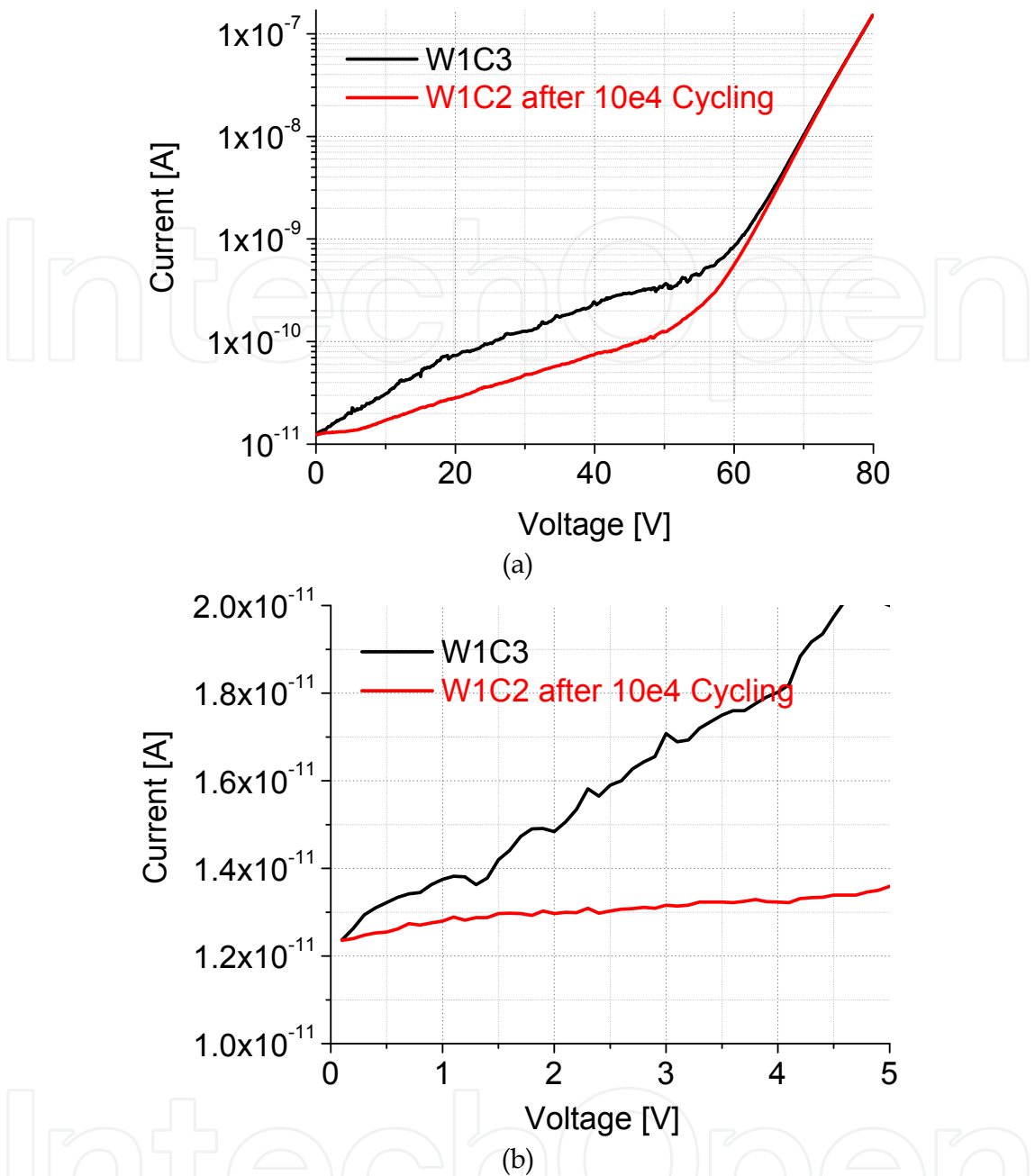


Fig. 23. Comparison between the I vs V curves of a sample in wafer #1 (Nitride) before (reference sample C3) and after (sample C2) imposing 10^4 cycles of a DC train at 50 V.

From the analysis of data plotted in Fig. 22 and in Fig. 23, it turns out that the response with poly-silicon is still affected by charge injection also after the described processing for $V_g > 5$ V, thus giving evidence for a residual contribution coming directly from the interface between doped poly-silicon and dielectric. In fact, the recorded curves are different with respect to the behaviour of MIMs manufactured by using top and bottom metal electrodes, because the poly-silicon electrodes are always characterized by a ramp behaviour in the first region. It is also worth noting that by using a DC train with a voltage value less than that needed for the charge injection onset (60 V), no shift is recorded (see Fig. 22). From the I vs V plots and from data recorded in Table 1, we can draw the following general conclusions:

The breakdown is not critical for structures with Poly-silicon electrodes. Usually $V_B \geq 100$ volt is measured. On the other hand the dielectric looks like not ideal, because a linear response of the current vs the applied voltage is recorded already at low voltage levels, thus demonstrating a not negligible resistive contribution of the bulk of the capacitor. Another possible mechanism for conduction could be due to the presence of Poly-silicon: the dielectric interface can probably be considered as a sort of MOS with a poly-silicon p-doped and a thin non-ideal dielectric layer.

Charging of the samples is obtained when successive ramps are applied, as evidenced from the shift of the I vs V characteristics when the measurement is repeated, in times shorter or in the order of one minute, in the same direction (positive or negative voltages). Moreover, the de-charging is very slow, and also after one day there is not a complete spontaneous restoring of the initial conditions.

Partial de-charging occurs when ramping the sample with positive and negative voltages, and re-combination of the charges is obtained, but the initial conditions are never re-obtained also by using this treatment.

The measured trend of the current is never ideal for the exploited samples, and a linear response is always obtained as a function of the applied voltage, while a constant value is expected for an almost ideal dielectric material. So far, the second term in Eq. (2) is always present. By cycling one sample with pulses as high as 50 V such a response is flattened, maybe due to the re-combination of residual charges belonging to defects of the material coming out from the technological process.

In the structures measured on wafer #7 to #11 some criticality in the measurements is evidenced, because of the small thickness of the metal contact, due to the pressure to be exerted by the probes.

In the case of the sample C3 belonging to wafer #1, with Si_3N_4 , a linear fit has been superimposed to the I vs V curve to evaluate the resistance of the sample. The result is presented in Fig. 24, from which it turns out a slope of $0.4 \times 10^{-11} \Omega^{-1}$, i.e. $R_a = 2.5 \times 10^{11} \Omega$.

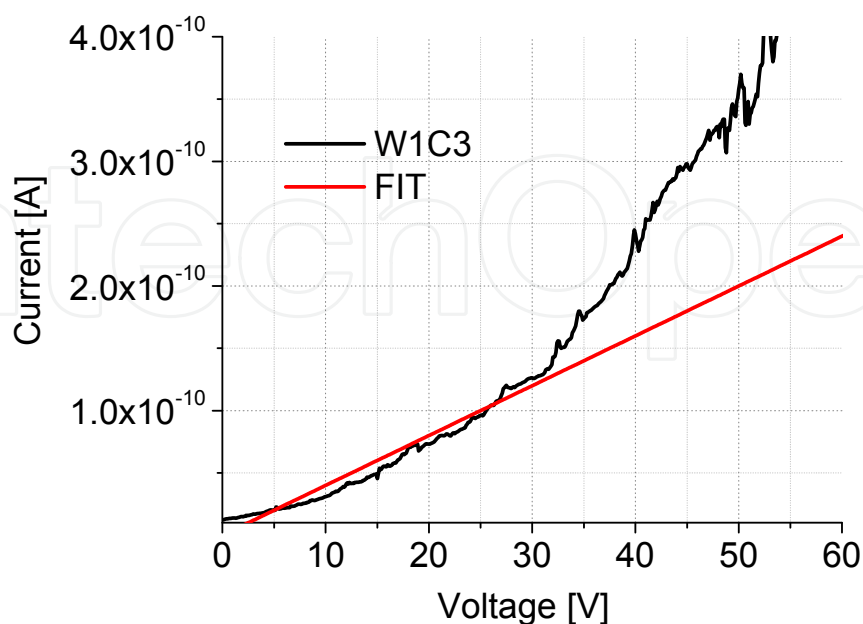


Fig. 24. Linear Fit to evaluate the resistance offered by the MIM material, namely Si_3N_4 , before the onset of the Poole-Frenkel effect. A slope of $0.4 \times 10^{-11} \Omega^{-1}$ is obtained.

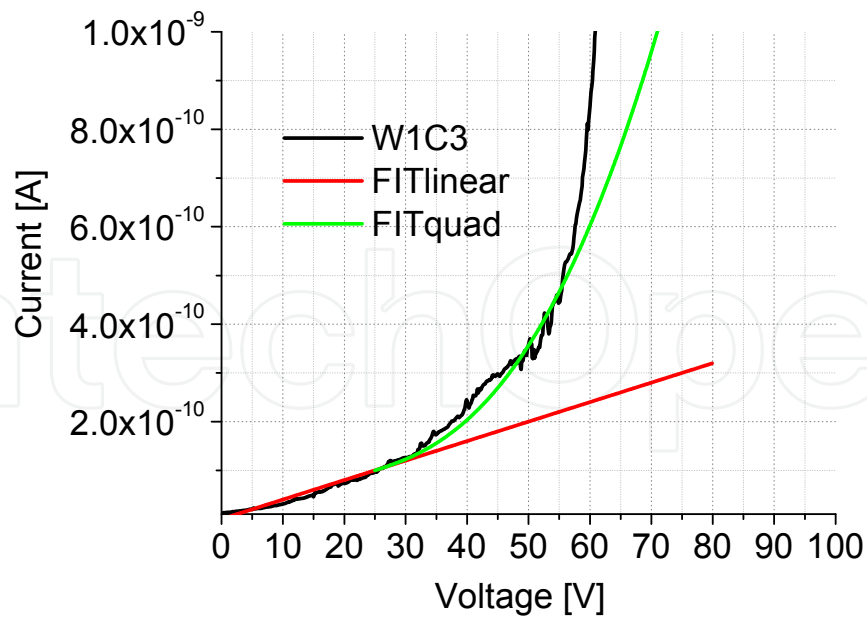


Fig. 25. Linear and quadratic fit for the measured current vs the applied voltage when the sample C3 belonging to wafer #1 (W1C3, Si₃N₄) is biased. Up to 25-30 V a linear dependence is obtained, while an almost quadratic law is found for $V_g > 25$ V.

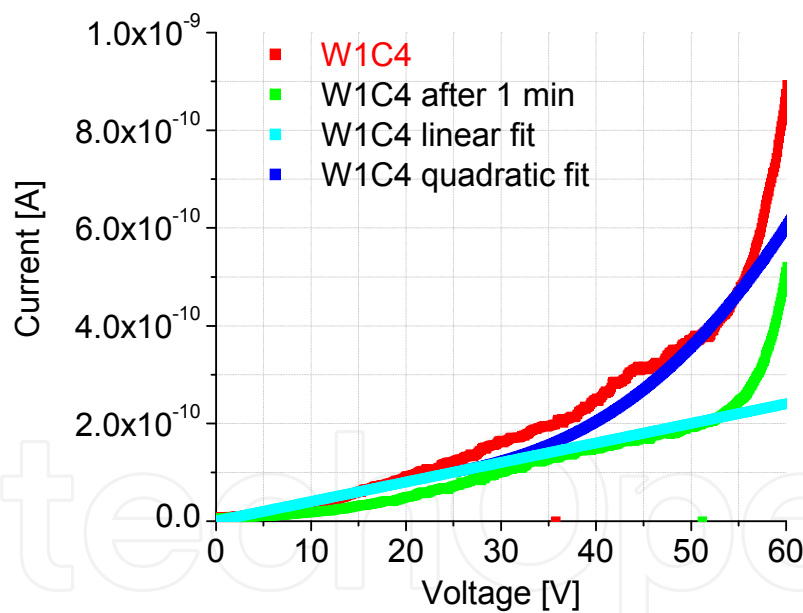


Fig. 26. Measurement of the C4 sample belonging to wafer #1. The red curve is for the first ramp imposed to the sample, and the green one is the response after the second ramp, one minute after the first one. The azure and blue curves refer to the linear and quadratic response respectively (low and high voltage values). The green curve is shifted due to the onset of the Poole-Frenkel effect, which lowers the current response at the same voltage.

Considering the area of the MIM $A=(440\times10^{-6})^2$ m² and the thickness $d=0.1\times10^{-6}$ m, the resistivity of the material will be $\rho=A\times R_a/d=4.84\times10^{11}$ Ω m, or $\sigma=2.07\times10^{-12}$ Ω^{-1} m⁻¹, thus confirming the high resistivity of the material, but a non-ideal response in terms of dielectric behavior [67].

Actually, in Figure 25, the linear fit is compared with the quadratic one, obtained by means of the formula $f(V_g) = 0.4 \times 10^{-11} V_g + 0.5 \times 10^{-13} (V_g - 25)^{2.5}$. This result is a correction with respect to the simple quadratic law in [61].

As a final comparison, the sample C4 in wafer #1 has been subjected to a measurement I vs V and fitted following the law $(V_g - 25)^{2.5}$. The result is shown in Fig. 26, where the displacement due to charging is evidenced, and it has to be attributed to the Poole-Frenkel Effect.

5. Dielectric polarization and Poole-Frenkel effect in RF MEMS and MIM

On the time scale of interest to the RF-MEMS capacitive switches response (i.e. greater than 1 μ sec) an electric field can interact with the dielectric film in two primary ways. These are: (i) the re-orientation of defects having an electric dipole moment, such as complex defects, and (ii) the translational motion of charge carriers, which usually involve simple defects such as vacancies, ionic interstitials and defect electronic species. These processes give rise to the dipolar (P_D) and the intrinsic space charge (P_{SC-i}) polarization mechanisms, respectively. Moreover, when the dielectric is in contact with conducting electrodes charges are injected through the trap assisted tunneling and/or the Poole-Frenkel effect [69] giving rise to extrinsic space charge polarization (P_{SC-e}) whose polarity is opposite with respect to the other two cases. In RF-MEMS capacitive switches during the actuation all the polarization mechanisms occur simultaneously and the macroscopic polarization is given by

$$P_{tot} = P_D + P_{SC-i} - P_{SC-e} \quad (4)$$

Now, from elementary physics it is known that the electric displacement D , defined as the total charge density on the electrodes, will be given by $D = \epsilon_0 E + P$, where E is the applied field and P the dielectric material polarization. The resulting polarization P may be further divided into two parts according to the time constant response [70]:

a) An almost instantaneous polarization due to the displacement of the electrons with respect to the nuclei. The time constant of the process is about 10^{-16} sec and defines the high frequency dielectric constant that is related to the refractive index.

b) A delayed time dependent polarization $P(t)$, which determines the dielectric charging in MEMS, starting from zero at $t=0$, due to the orientation of dipoles and the distribution of free charges in the dielectric, the dipolar and space charge polarization respectively. Moreover the growth of these polarization components may be described in the form of

$P_j(t) = P_{j0} \cdot [1 - f_j(t)]$. The index j refers to each polarization mechanisms, and $f_j(t)$ are exponential decay functions of the form $\exp\left[-\left(\frac{t}{\tau}\right)^\beta\right]$. Here τ is the process time and β the

stretch factor. If $\beta=1$ the charging/discharging process is governed by the Debye law. In disordered systems like the amorphous oxides, which possess a degree of disorder, $\beta < 1$ and the charging/discharging process is described by the stretched exponential law.

In the case of a MEMS switch that operates under the waveforms in Fig. 4, the dielectric is subjected to charging when the bridge is in the DOWN position and discharging in the UP position, independently of the ON or OFF functionality of the device. More specifically, when a uni-polar pulse train is applied (Fig. 4 (a)) then the device is subjected to contact-less

charging below pull-in and pull-out. Above pull-in and pull-out the device is subjected to contact charging.

If we assume that at room temperature the density of free charges in the LTO, i.e. SiO₂ deposited at low temperature, is very low we can re-write Eq. (4) as:

$$P = P_D - P_{SC} \quad (5)$$

where P_{SC} is the space charge polarization of extrinsic origin. When we apply a pulse train the following will occur:

- during the contact-less charging the electric field increases the dipolar polarization and assists to re-distribution and dissipation of injected charges
- during the contact charging the high electric field causes a further increase of the dipolar polarization, and through the charge injection contributes to the build-up of space charge polarization

Due to the dielectric film polarization the pull-in and pull-out voltages will be determined by:

$$V_{pi} = \sqrt{\frac{8kz^3}{27\varepsilon_0 A} - \frac{z_1 P_{pi}}{\varepsilon_0}} ; V_{po} = \sqrt{\frac{2kz_1^2(z - z_1)}{\varepsilon_0 A} - \frac{z_1 P_{po}}{\varepsilon_0}} \quad (6)$$

In the Si₃N₄ dielectric it has been shown that, at room temperature, the space charge polarization induced by the charge injection is the dominant mechanism [71][72]. If we assume that the same effect holds for SiO₂ we are led to the conclusion that the pull-out voltage will increase with time when a uni-polar pulse train is applied.

The dependence of the actuation and de-actuation voltages on the number of cycles was fitted for the exploited RF MEMS devices S1 and CL studied in the previous sections, by assuming that the charging process follows the stretched exponential law.

The fitting of data has been performed as a function of the number of cycles (N), since each cycle maintains a constant shape and represents a certain effective ON and OFF time. This is particularly useful in actual devices, when the reliability can be determined by the number of total actuations as well as the total time during which the RF MEMS switch remains actuated. The differences in the effective ON and OFF times will reflect in the number of cycles (N^*) that corresponds to the process time τ . According to Eq. (6), and in agreement with the above discussed growth for the polarization, we can apply the following equation to describe the evolution of the pull-in and pull-out voltages as a function of time/number of cycles.

$$V_j(N) = V_{0,j} - \frac{z_1 P_j}{\varepsilon_0} \cdot \left\{ 1 - \exp \left[- \left(\frac{N}{N_j^*} \right)^\beta \right] \right\} \quad (7)$$

where z_1 is the dielectric thickness, j an index that stands for actuation (pull-in) and de-actuation (pull-out) while $V_{0,j}$ represents the pull-in and pull-out voltages that are determined by the electro-mechanical model.

The fitting results show excellent agreement with the experimental data, and the fitting parameters are listed in Table 2, with reference to Fig. 5 and Fig 6 of the current contribution.

Here it must be pointed out that:

$$\Delta V = -\frac{z_1 P_j}{\epsilon_0} = -\frac{z_1 \cdot (P_{D,j} - P_{SC,j})}{\epsilon_0}$$

(8)

		V ₀	ΔV	β	N*
Fig. 5	Act	13.5	54.4	0.69	1.67
	Deact	29.5	33.2	0.96	1.96
Fig. 6	Act	27.0	54.5	1	1.67
	Deact	36.8	22.4	0.83	2.5

Table 2. Fitted values for the exponential trend of the actuation (Act) and de-actuation (Deact) of both S1 and CL devices.

The fitting results reveal that the dominant mechanism is the space charge polarization ($P_j<0$). Moreover, it is worth noting that the actuation voltage increases faster than the de-actuation one. Such a behavior can result from a faster increase of space charge polarization or decrease of dipolar polarization when the bridge is non-actuated. Taking into account that the dipolar polarization in SiO₂ is characterized by long time constants (fig. 4 of [72]), we are led to the conclusion that the differences in the increase of actuation and de-actuation voltages arise from the mechanisms involved in charge injection and collection, respectively. This can be easily understood if we bear in mind that the charge injection occurs under high electric field and that the trap assisted tunneling charging process gives rise to a spatial distribution of charges in the vicinity of the injecting contacts. During the OFF state, where no bias is applied, the trapped charges (located at the dielectric free surface) are emitted and finally collected by the bottom electrode. The charge collection, which takes place through diffusion and drift in the presence of local electric fields, is complex owing to multi trapping processes. Regarding the charges that are injected from the bottom electrode, they are collected much sooner than the top ones. Moreover, these charges have a small influence on the dielectric polarization.

Another possible situation could be the charging between the actuation pads and the ground plane of CPW across the substrate dielectric [73]. This charging process gives rise to a longitudinal polarization across the substrate oxide that behaves like the dipolar polarization. The values of N^* for actuation and de-actuation agree with the presence of both mechanisms, which is a slower build-up of space charge polarization and competition from a longitudinal polarization across substrate.

Applying a bipolar bias scheme we observe that both actuation and de-actuation voltages do not vary significantly with time, as it is also the case for other recently considered RF MEMS switch configurations, like the miniature one [74]. This can be easily attributed to the field induced charging/discharging processes. A significant difference that arises from the bipolar actuation is the reversal of magnitude of actuation and de-actuation voltages. This behavior has been occasionally observed but not investigated in depth. If we take into account that in MEMS switches the charging is asymmetric, a reason that leads to stiction even under bipolar actuation, we may assume that this effect is probably responsible for the observed reversal. In such a case the value of P_{po} will change polarity and magnitude after each change of the actuation voltage polarity. In any case the observed behavior is under investigation.

Concerning the charging effects in a MIM capacitor, let’ analyse as an example experimental results based on silicon dioxide deposited by means of a low temperature process (LTO=low temperature oxide), as it is shown in Fig. 19 (a).

The MIM was made by a poly-silicon layer as the bottom electrode, with metal on the top side (top electrode) and LTO as a dielectric layer. The structure emulates the situation of a fully collapsed bridge by means of a lateral actuation, where poly-silicon is used as the material for the feeding lines and for the pad under bridge, while LTO is deposited on the top of it to provide an electrical isolation; the metal on the top is equivalent to the bridge touching the actuation electrode when the voltage is applied. Such an arrangement, i.e. a multilayer polysilicon/dielectric/metal, is also a source of further injection of charges, because polysilicon is not just a bad conductor and it can also contribute at the interface polysilicon/dielectric. The sample was measured by repeating a slow voltage ramp three times and measuring the corresponding current. In particular, a ramp rate $dV/dt=0.05$ V/sec and a maximum voltage of 80 volt were imposed. As expected, the charging process is enhanced, and this is evidenced by the current drop after each ramp, but the effect is less important the third time, thus demonstrating the saturation of the charge injected in the sample, as also experienced in the real MEMS switches already discussed in this paper. As already outlined, the measured trend of the current is not ideal for the exploited sample and for similar ones based on silicon nitride, and a linear response is always obtained as a function of the applied voltage, while a constant value is expected for an almost ideal dielectric material at low voltage values, i.e. in a range up to, at least, 20-25 volt for typical dielectric materials used in microelectronics. The same data of Fig. 19 (a) have been plotted in Fig. 27, by using I/V vs $V^{1/2}$, to check the Poole-Frenkel effect. Actually, the current dependence on bias seems to be determined by the Poole-Frenkel effect when the applied bias exceeds the value of 50 volt:

$$I(V) = I_0 E \exp\left(b_{PF}^* \sqrt{E} - \frac{\Phi_n}{kT}\right) \text{ where } b_{PF}^* = \frac{1}{kT} \sqrt{\frac{q^3}{\pi \epsilon \epsilon_0}} \tag{9}$$

The change of b_{PF} in SiN has been investigated by S.P. Lau et al. and attributed to large concentration of defects in SiN and the formation of defect band. Taking into account the increase of b_{PF} with the applied electrical stress we are led to the conclusion that the latter decreases the density of traps in the SiN film [75].

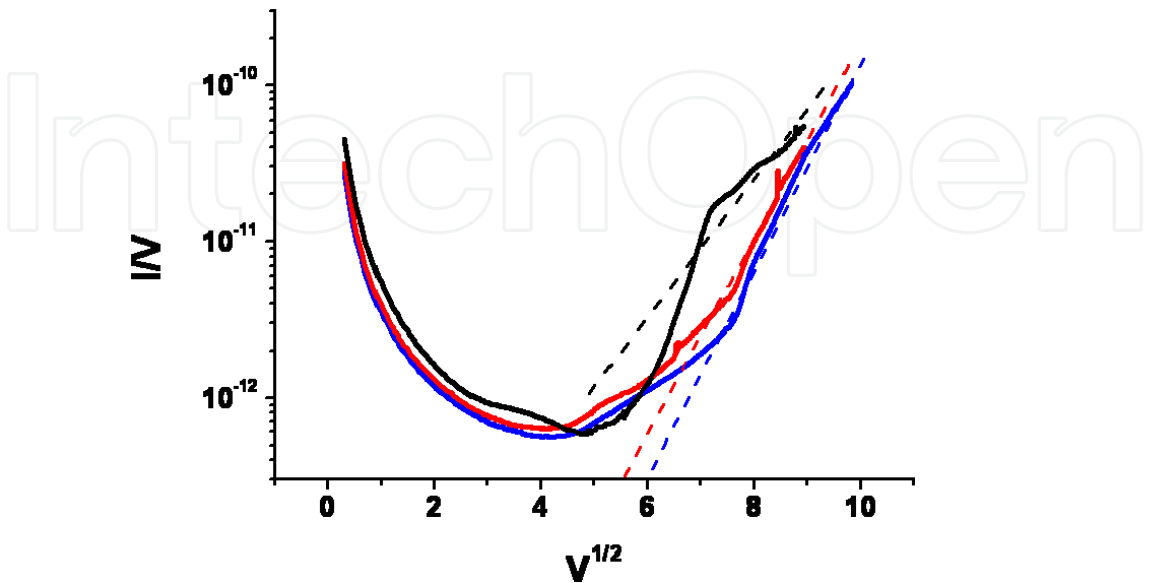


Fig. 27. I/V curve as a function of the $V^{1/2}$ by using data from Fig. 19 (a).

To better investigate this aspect, an additional characterization was performed on a sample with the same structure for the bottom and for the top electrodes and with Si_3N_4 as dielectric. Two samples have been measured: (i) the first one in the usual way, by means of a slow voltage ramp, and (ii) another one by imposing a typical stress used for the switches, subjecting it to a high number of DC pulses and measuring the characteristic current vs voltage after that. Actually, 10^4 pulses with a pulse-width $\tau = 250$ ms and with a period $T = 500$ ms (duty cycle = $\tau/T = 50\%$), with a voltage $V=50$ volt, have been used. As a result, the low voltage response has been “rectified” as it is shown in Fig. 28, where the initial behavior is almost constant, as expected by a dielectric material without free charges incorporated. We believe that such a trend can be justified by the neutralization of surface free charges at the interface between the dielectric layer and the top metal, where, due to the roughness, charges are trapped but free to contribute when a DC field is imposed. The energy released by the DC input pulses, provided quickly with respect to the time constants for the material de-charging, was high enough to favor the re-combination of the charges, thus locally improving the quality of the dielectric material.

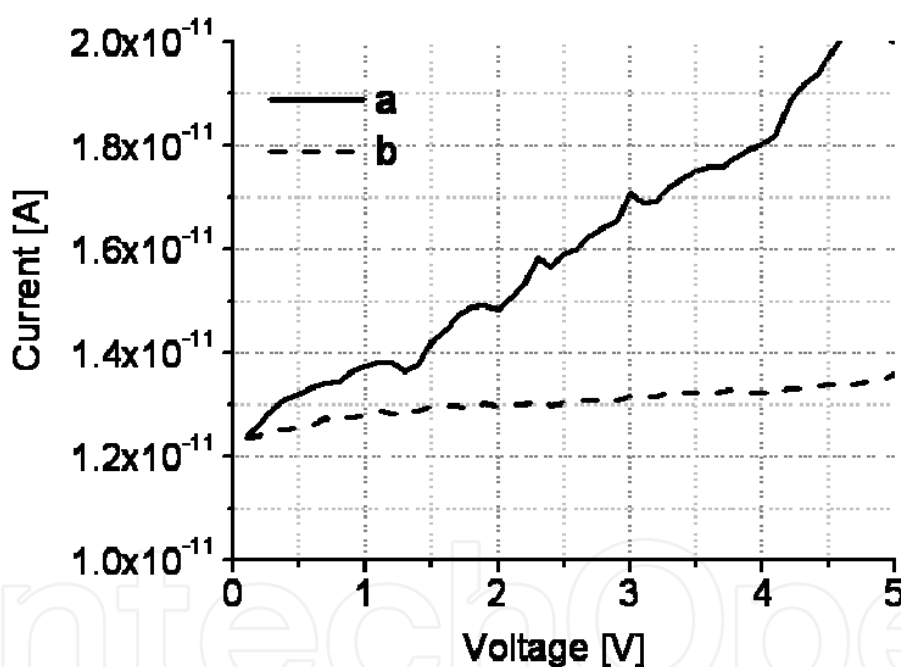


Fig. 28. Measured trend of the current as a function of the applied voltage for a MIM made by Si_3N_4 before (curve a) and after (curve b) cycling the sample with pulses as high as 50 volt. Generally, a linear response is always obtained as a function of the applied voltage, while a constant value is expected for an almost ideal dielectric material. By cycling the sample such a response is flattened, maybe due to the re-combination of residual charges belonging to defects of the material surface coming out from the technological process. Actually, a comparison has been done between the charging response of MIM capacitors and RF MEMS switches, and the differences coming from such an analysis have been discussed with emphasis on the different times needed for re-storing the initial conditions or for preventing the charging itself.

6. Conclusion

In conclusion, this chapter has been organized describing the technological aspects for manufacturing both MIMs and RF MEMS switches, and discussing, on the base of several experimental findings, the theoretical framework for the interpretation of the measured charging effects. In particular, the theoretical approach for charging occurring in the exploited devices has been based on the Poole-Frenkel effect and it has been related to the involved polarization mechanisms. Many structures have been studied, looking for the most promising ones to be used for the actuation of RF MEMS switches, minimizing the charging effects.

Two configurations of RF MEMS switches using electrostatic actuation, and several MIMs devices simulating the RF MEMS actuation pads, with various dielectric materials and electrodes, have been measured.

As experienced in the RF MEMS measurements, and well established in literature, the charge stored in the dielectric material used for the actuation pads creates an electric field that is always opposite with respect to the electric field generated by the actuation voltage. This is evident in the case of an uni-polar actuation signal, with an increase in the actuation voltage for the switch, and it was confirmed in our measurements.

Mainly, charging is responsible for sticking, and it is also related to the increase of the actuation voltage, especially under uni-polar DC biasing. By using lower actuation voltages or a bi-polar scheme this effect is more under control and compliant with ground and space applications, which should not overcome 50 volt of bias to be really appealing in several sub-systems.

The process necessary to trap and de-trap the carriers in the uni-polar scheme can be described mainly by the Poole-Frenkel effect; it is very slow, and the initial conditions for the device should need long times to re-obtain the same actuation voltage. To accelerate the restoring mechanism, a bi-polar actuation scheme was applied to the same devices, and from the experiment it turns out that the gradient experienced by the switch under test helps a faster de-trapping mechanism, giving back the initial value of the actuation conditions. Actually, the voltage difference necessary for the successive actuations in the bi-polar scheme is always constant and the absolute value of the actuation and de-actuation voltages too, at least for a limited number of actuations.

For the MIM structures, a comparison has been performed between different materials and electrodes to simulate the RF MEMS actuation pads. From the measurements, it turns out that the change of interface and of the dielectric material, as well as the deposition technique used for obtaining the dielectric layer, are critical choices to activate charging mechanisms.

The breakdown is not critical for structures with Poly-silicon electrodes. Usually $V_B \geq 100$ V is measured, while metal bottom electrodes have $V_B \leq 50$ -60 V. On the other hand all the exploited dielectric materials look like not ideal, as a linear response of the current Vs the applied voltage is recorded already at low voltage levels, thus demonstrating a not negligible resistive contribution of the bulk of the capacitor. Another possible mechanism for conduction could be the presence of Poly-silicon: the dielectric interface can probably be considered as a sort of MOS with a poly-silicon p-doped and a thin non-ideal dielectric layer.

Charging of the samples is obtained when successive ramps are applied, as evidenced from the shift of the I Vs V characteristics by means of the application of positive and negative voltages. Moreover, the de-charging of the MIM is very slow, and also after one day there is

not a complete spontaneous restoring of the initial conditions, against the previous finding for RF MEMS switches. *This could be an evidence that the charging effects occurring in the actual MEMS device cannot be completely emulated by a MIM structure, as the times for restoring the initial conditions are quite different between them. Anyway, in spite of a possible indication for different processes, due to the actuation itself, the charging properties of the material used for the actuation pads will be always present.* In the case of the measured switches, TEOS was used for the actuation pads, which exhibits quite pronounced charging effects as evidenced also in MIM structures (see Fig. 16).

Moreover, better performances in the I Vs V response can be obtained when the MIM is subjected to several pulses, analogously to those used in operating conditions for RF MEMS, maybe due to recombination of charges (left free from the technological process) when subjected to such an electrical stress.

Concerning the materials and the deposition techniques, from the results shown in Table 1 and from the plots is difficult to draw a final conclusion, but one can see that generally Si_3N_4 exhibits an almost linear response for the current as a function of the applied voltage in a voltage range wider with respect to SiO_2 (LTO, TEOS). Moreover, the PECVD HF Nitride deposited at 300 °C looks like better also in terms of current reversal with respect to TEOS, and it is attributed to a higher densification temperature (Fig. 21). Actually, charge injection is present in both materials owing to the non-ideal response of the I Vs V curve, which should be flat at low voltages, but a strong non-linear behaviour due to the Poole-Frenkel effect is obtained only for $V > 50\text{-}60$ V for Si_3N_4 and for $V > 20\text{-}30$ V for SiO_2 .

7. Acknowledgment

Work partially funded by the European Space Agency (ESA) Contract 20847/07/NL/GLC “High Reliability MEMS Redundancy Switch”.

Adriano Cola from CNR-IMM Lecce and Luigi Mariucci from CNR-IMM Roma are kindly acknowledged for helpful discussions on charge effects in MIM structures.

8. References

- [1] Hopkinson, J.; Wilson, E. On the capacity and residual charge of dielectrics as affected by temperature and time. *Phil. Trans. Roy. Soc. London. A* 1897, 189, 109-135.
- [2] Binet, G.; Freire, M.; Van Eesbeek, M.; Daly, E.; Drolshagen, G.; Henriksen, T.; Thirkettle, A.; Poinas, P.; Eiden, M.; Guglielmi, M. *Space specifications check list*; ESA-ESTEC: Noordwijk, Netherlands, 2006, https://iti.esa.int/iti/resource/Space_Specifications_Checklist.doc.
- [3] Asokan, T. Ceramic dielectrics for space applications. *Curr. Sci.* 2000, 79, 348-351.
- [4] Nguyen, C.T.-C.; Katehi, L.P.B.; Rebeiz, G.M. Micromachined devices for wireless communications. *Proc. IEEE* 1998, 86, 1756-1768.
- [5] De Los Santos, H.J. *Introduction to Microelectromechanical (MEM) Microwave Systems*, Artech House, Boston, 1999.
- [6] Senturia, S. *Microsystem Design*, Springer, New York, 2001.
- [7] De Los Santos, H.J. *RF MEMS Circuit Design for Wireless Communications*, Artech House, Boston, 2002.
- [8] Rebeiz, G. M. *RF MEMS Theory, Design, and Technology*, 1st Ed.; John Wiley & Sons: Hoboken, New Jersey, USA, 2003.

- [9] Maluf, N.; Williams, K. *An Introduction to Microelectromechanical Systems Engineering*, 2nd Ed.; Artech House, Boston, 2004.
- [10] Joung, J.; Shen, J.; Grodzinski, P. Micropumps based on alternating high-gradient magnetic fields. *IEEE Trans. Magn.* 2000, 36, 2012–2014.
- [11] Yan D.; *Mechanical Design and Modeling of MEMS Thermal Actuators for RF Applications*, thesis on Master of Applied Science in Mechanical Engineering, http://resonance.uwaterloo.ca/students/dyan/thesis_winter_master.pdf, Waterloo, Ontario, 2002
- [12] Lee, H.-C.; Parkand, J.-Y.; Bu, J.-Uk. Piezoelectrically Actuated RF MEMS DC Contact Switches With Low Voltage Operation *IEEE Microwave and Wireless Components Lett*, 2005, 15, 202–204.
- [13] De Los Santos, H.; Fischer, G.; Tilmans, H.A.C.; van Beek, J.T.M. RF MEMS for Ubiquitous Wireless Connectivity Part 1-Fabrication and Part 2-Application. *IEEE Microwave Magazine*, 2004, 5, 36–65
- [14] ESA/ESTEC Project No. 14628/NL/CK-MEM Switch on: MICROWAVE ELECTROSTATIC MICRO-MACHINED DEVICES FOR ON-BOARD APPLICATIONS
- [15] ESA-ESTEC Project MEDINA No. 14627/00/NL/WK
- [16] Fernández-Bolaños, M.; Lisec, T.; Dainesi, P.; Ionescu, A. M. Thermally Stable Distributed MEMS Phase Shifter for Airborne and Space Applications. *Proceedings of the 38th European Microwave Conference*, 2008, October 2008, Amsterdam, The Netherlands, 100–103.
- [17] Dussopt, L.; Rebeiz, G. M. Intermodulation distortion and power handling in RF MEMS switches, varactors, and tunable filters. *IEEE Trans. Microw Theory Tech.*, 2003, 51, 1247–1256.
- [18] Girbau, D.; Otegi, N.; Pradell, L. Study of Intermodulation in RF MEMS Variable Capacitors. *IEEE Trans. Microw Theory Tech.*, 2006, 54, 3, 1120–1130.
- [19] Mercier, D.; Blondy, P.; Barataud, D.; Cros, D.; Guillon, P.; Champeaux, C.; Tristant, P.; Catherinot, A. Model for MEMS Switches Power Handling and Phase Noise. *Proc. of the European Microwave Week 2002*, Milano, Italy, 1–4.
- [20] Peroulis, D.; Pacheco, S. P.; Katehi, L. P. B. RF MEMS Switches With Enhanced Power-Handling Capabilities. *IEEE Trans. Microw Theory Tech.*, 2004, 52, 50–68.
- [21] Choi, Joo-Young; Ruan, Jinyu; Coccetti, Fabio; Lucyszyn, Stepan, Three-Dimensional RF MEMS Switch for Power Applications, *IEEE Trans. on Ind. Electronics*, Vol. 56, No. 4, April 2009, 1031–1039.
- [22] Mardivirin, D.; Pothier, A.; Orlianges, J.C.; Crunteanu, A.; Blondy, P. Charging Acceleration in Dielectric Less RF MEMS Switched Varactors under CW Microwave Power, *Proc. of Int. Microwave Symposium*, 2009.
- [23] TERAVIDTA DATA Sheet on “SP4T 7GHz RF MEMS Switch”, http://www.teravicta.com/site/images/pdf/TT1414/DS-TT1414_1.3.pdf (2007).
- [24] Di Nardo, S.; Farinelli, P.; Giacomozzi, F.; Mannocchi, G.; Marcelli, R.; Margesin, B.; Mezzanotte, P.; Mulloni, V.; Russer, P.; Sorrentino, R.; Vitulli, F.; Vietzorreck, L. Broadband RF-MEMS Based SPDT; In *Proceedings of the 36th Microwave Conference*, Manchester, UK, 10–15, September 2006; pp. 1727 – 1730.

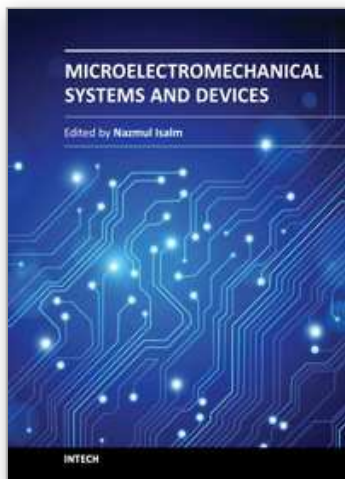
- [25] McErlean, E.P.; Hong, J.-S.; Tan, S. G.; Wang, L.; Cui, Z.; Greed, R. B.; Voyce, D.C. 2x2 RF MEMS switch matrix. *Microwaves, Antennas and Propagation, IEE Proceedings* 2005, 449 – 454.
- [26] Catoni, S.; Di Nardo, S.; Farinelli, P.; Giacomozzi, F.; Mannocchi, G.; Marcelli, R.; Margesin, B.; Mezzanotte, P.; Mulloni, V.; Pochesci, D.; Sorrentino, R.; Vitulli, F.; Vietzorreck, L.: RF MEMS Matrices for Space Applications, In Proceedings of the 2007 MEMSWAVE Workshop, 8th International Symposium on RF MEMS and RF Microsystems, Barcelona, Spain, 26-29 June 2007.
- [27] Barker, S.; Rebeiz, G. M. Distributed MEMS true-time delay phase shifters and wide-band switches, *IEEE Trans. Microw Theory Tech.*, 1998, 46, 1881-1890
- [28] Buttiglione, R.; Dispenza, M.; Fiorello, A. M.; Tuominen, J.; Kautio, K.; Ollila, J.; Jaakola, T.; Rönkä, K.; Catoni, S.; Pochesci, D.; Marcelli, R. Fabrication of high performance RF-MEMS structures on surface planarised LTCC substrates. In Proceedings of EMPC2007, European Microelectronics and Packaging Conference and Exhibition , Oulu, Finland, 17-20 June, 2007.
- [29] Rebeiz, G. M.; Tan, G.-L.; Hayden, J. S. RF MEMS Phase Shifters: Design and Applications. *IEEE Microwave Magazine*, 2002, 3,72-81.
- [30] Bartolucci, G.; Catoni, S.; Giacomozzi, F.; Marcelli, R.; Margesin, B.; Pochesci, D. Realization of a distributed RF MEMS Phase Shifter with a very low number of switches. *Electron. Lett.*, 2007, 43, 1290 - 1291.
- [31] Zhou, L.; RF MEMS DC Contact Switches for Reconfigurable Antennas. Thesis on Master of Science in Electrical Eng., San Diego State University, http://digitaladdis.com/sk/Lei_Zhou_Thesis_RF_MEMS.pdf (2006)
- [32] Kornumpf, W. P.; Karabudak, N. N.; Taft, W. J. RF MEMS PACKAGING FOR SPACE APPLICATIONS. In Proc. of 22nd AIAA International Communications Satellite Systems Conference & Exhibit, Monterey, California, 9 - 12 May 2004.
- [33] Goldsmith, C.; Ehmke, J.; Malczewski, A.; Pillans, B.; Eshelman, S.; Yao, Z.; Brank, J.; Eberly, M.; Lifetime characterization of capacitive RF MEMS switches. *Proc. of IEEE MTTS Int Microw Symp*, 2001, 227-230.
- [34] Yuan, X.; S. Cherepko, V. J.; Hwang, C. M.; Goldsmith, C. L.; Nordquist, C.; Dyck C. Initial observation and analysis of dielectric-charging effects on RF MEMS capacitive switches, *Proc. of IEEE MTTS Int Microw Symp*, 2004, 1943-1946.
- [35] Van Spengen, W.M.; Puers, R.; Mertens, R.; De Wolf, I. A comprehensive model to predict the charging and reliability of capacitive RF MEMS switches *J. Micromech. Microeng.* 2004, 14, 514-521.
- [36] Patton, S. T.; Zabinski, Jeffrey, S. Effects of dielectric charging on fundamental forces and reliability in capacitive microelectromechanical systems radio frequency switch contacts. *J. Appl. Phys.*, 2006, 99, 94910-94910-11
- [37] Peng, Z.; Yuan, X.; Hwang, J. C. M.; Forehand, D. I.; Goldsmith, C. L. Superposition Model for Dielectric Charging of RF MEMS Capacitive Switches Under Bipolar Control-Voltage Waveforms *IEEE Trans. Microw Theory Tech.*, 2007, 55, 2911-2918.
- [38] Peng, Z.; Palego, C.; Hwang, J. C. M.; Moody, C.; Malczewski, A.; Pillans, B. W.; Forehand, D. I.; Goldsmith, C.L. Effect of Packaging on Dielectric Charging in RF MEMS Capacitive Switches *Proc. of IEEE MTTS Int Microw Sym.*, 2009, 1637-1640.
- [39] Marcelli, R.; Papaioannu, G.; Catoni, S.; De Angelis, G.; Lucibello, A.; Proietti, E.; Margesin, B.; Giacomozzi, F.; Deborgies, F.; Dielectric Charging in Microwave

- Micro-electro-mechanical Ohmic Series and Capacitive Shunt Switches. *J Appl Phys* 2009, 105, 114514-1 - 114514-10.
- [40] Wang, G.; *RF MEMS Switches with Novel Materials and Micromachining Techniques for SOC/SOP RF Front Ends* thesis on School of Electrical and Computer Engineering of the Georgia Institute of Technology, <http://smartech.gatech.edu/handle/1853/14112> 2006.
- [41] Theonas, V. G.; Exarchos, M.; Konstantinidis, G.; Papaioannou, G.J. RF MEMS sensitivity to electromagnetic radiation. *J Phys* 2005, *Conference Series* 10, 313-316
- [42] Tazzoli, A.; Peretti, V.; Autizi, E.; Meneghesso, G. EOS/ESD Sensitivity of Functional RF-MEMS Switches, *Proc. of EOS/ESD Symposium* 2008, 272-280
- [43] Ruan, J.; Papaioannou, G.J.; Nolhier, N.; Bafleur, M.; Coccetti, F.; Plana, R. ESD Stress in RF-MEMS Capacitive Switches: The Influence of Dielectric Material Deposition Method *IEEE CFP09RPS-CDR 47th Annual International Reliability Physics Symposium*, Montreal, 2009, 568-572
- [44] Papandreou, E.; Lamhamdi, M.; Skoulikidou, C.M.; Pons, P.; Papaioannou, G.; Plana, R.; Structure dependent charging process in RF MEMS capacitive switches. *Microelectron Reliab* 2007, 47, 1812-1817.
- [45] Mardivirin, D.; Pothier, A.; Crunteanu, A.; Vialle, B.; Blondy, P. Charging in Dielectricless Capacitive RF-MEMS Switches, *IEEE Trans. on Microwave Theory and Tech.*, Vol. 57, No. 1, January 2009, 231-236.
- [46] Peng, Z.; Palego, C.; Halder, S.; Hwang, J. C. M.; Jahnes, C. V.; Etzold, K. F.; Cotte, J. M.; Magerlein, J. H. Dielectric Charging in Electrostatically Actuated MEMS Ohmic Switches, *IEEE Trans. on Device and Materials Reliability*, Vol. 8, No. 4, December 2008, 642-646.
- [47] Yuan, X.; Peng, Z.; Hwang, J. C. M.; Forehand, D.; Goldsmith, C. L. Acceleration of Dielectric Charging in RF MEMS Capacitive Switches, *IEEE Trans. on Device and Materials Reliability*, 2006, 6, 556-563.
- [48] Zaghloul, U. ; Belarni, A. ; Coccetti, F.; Papaioannou, G.J.; Bouscayrol, L.; Pons, P.; Plana, R. A Comprehensive Study for Dielectric Charging Process in Silicon Nitride Films for RF MEMS Switches using Kelvin Probe Microscopy, *Proc. of Transducers* 2009, Denver, CO, USA, June 21-25, 2009, 789-793.
- [49] Broué, A.; Dhennin, J.; Segueineau, C.; Lafontan, X.; Dieppedale, C.; Desmarres, J.-M.; Pons, P.; Plana, R. Methodology to Analyze Failure Mechanisms of Ohmic Contacts on MEMS Switches *Proc. of IEEE CFP09RPS-CDR 47th Annual International Reliability Physics Symposium*, Montreal, 2009, 869-873.
- [50] Czarnecki, P.; Rottenberg, X.; Soussan, P.; Nolmans, P.; Ekkels, P.; Muller, P.; Tilmans, H.A.C.; De Raedt, W.; Puers, R.; Marchand, L.; De Wolf, I. New Insights into Charging in Capacitive RF MEMS Switches *Proc. of IEEE CFP08RPS-CDR 46th Annual International Reliability Physics Symposium*, Phoenix, 2008, 496-505.
- [51] Richard Daigler, Eleni Papandreou, Matroni Koutsourelis, George Papaioannou, John Papapolymerou, Effect of deposition conditions on charging processes in SiNx: Application to RF-MEMS capacitive switches, *Microelectronic Engineering* 86 (2009) 404-407.
- [52] Romolo Marcelli, Giancarlo Bartolucci, George Papaioannu, Giorgio De Angelis, Andrea Lucibello, Emanuela Proietti, Benno Margesin, Flavio Giacomozzi, François

- Deborgies, Reliability of RF MEMS Switches due to Charging Effects and their Circuitual Modelling, *Microsystem Technologies*, Vol. 16, pp. 1111-1118 (2010).
- [53] Catoni, S.; Di Nardo, S.; Farinelli, P.; Giacomozzi, F.; Mannocchi, G.; Marcelli, R.; Margesin, B.; Mezzanotte, P.; Mulloni, V.; Sorrentino, R.; Vitulli, F.; Vietzorreck, L. Reliability and Power Handling Issues in Ohmic Series and Shunt Capacitive RF MEMS Switches *Proceedings of the 2006 MEMSWAVE Workshop*, 7th International Symposium on RF MEMS and RF Microsystems, Orvieto, Italy, 26-29 June, 2006.
- [54] Melle, S.; De Conto, D.; Mazenq, L.; Dubuc, D.; Poussard, B.; Bordas, C.; Grenier, K.; Bary, L.; Vendier, O.; Muraro, J.L.; Cazaux, J.L.; Plana, R. Failure Predictive Model of Capacitive RF-MEMS. *Microelectron Reliab* 2005, 45, 1770-1775.
- [55] Vandershueren, J. and J. Casiot in *Thermally stimulated relaxation in solids*; Braunlich, P. (Ed.); Springer-Verlag, Berlin, Germany, 1979, volume 37
- [56] Papaioannou, G.; Papapolymerou, J.; Pons, P.; Plana, R.; *Appl Phys Lett* 2007, 90, 233507
- [57] Papaioannou, G.; Giacomozzi, F.; Papandreou, E.; Margesin, B.; Charging Processes in RF-MEMS Capacitive Switches with SiO₂ Dielectric *Proceedings of the 2007 MEMSWAVE Workshop*, 8th International Symposium on RF MEMS and RF Microsystems, Barcelona, Spain, 26-29 June 2007.
- [58] Czarnecki, P.; Rottenberg, X.; Soussan, P.; Ekkels, P.; Muller, P.; Nolmans, P.; De Raedt, W.; Tilmans, H.A.C.; Puers, R.; Marchand, L.; De Wolf, I.; Influence of the substrate on the lifetime of capacitive RF MEMS switches. *Proc. MEMS-2008*.
- [59] Xiaobin, Y.; Zhen, P.; Hwang, J.C.M.; Forehand, D.; Goldsmith, C.L.; A transient SPICE model for dielectric-charging effects in RF MEMS capacitive switches *IEEE Transactions on Electron Devices*, 2006, 53, 2640 - 2648.
- [60] Melle, S.; De Conto, D.; Mazenq, L.; Dubuc, D.; Poussard, B.; Bordas, C.; Grenier, K.; Bary, L.; Vendier, O.; Muraro, J.L.; Cazaux, J.L.; Plana, R. Failure Predictive Model of Capacitive RF-MEMS *Microelectron Reliab* 2005, 45, 1770-1775.
- [61] Franclov´a, J.; Ku´cerov´a Z.; Bur´s´ikov´, V.; Electrical Properties of Plasma Deposited Thin Films *WDS'05 Proceedings of Contributed Papers*, 2005, Part II, 353-356.
- [62] Harrell, W.R.; Frey, J.; Observation of Poole-Frenkel effect saturation in SiO₂ and other insulating films, *Thin Solid Films*, 1999, 352, 195-204.
- [63] Lamhamdi, M.; Guastavino, J.; Bpudou, L.; Segui, Y.; Pons, P.; Bouscayrol L.; Plana, R. Charging-Effects in RF Capacitive Switches Influence of insulating layers composition, *Microelectron Reliab* 2006, 46, 1700-1704.
- [64] Gupta, D. K.; Doughty, K.; Brockley, R.S. Charging and discharging currents in polyvinylidene fluoride, *J Phys D Appl Phys* 1980, 13, 2101-2114.
- [65] Wigner, E. On the constant A in the Richardson's Equation. *Phys. Review*, 1936, 49, 696-700
- [66] Schug, J. C.; Lilly A. C.; Lowitz, D. A. Schottky Currents in Dielectric Films, *Phys. Rev. B*, 1970, 1, 4811-4818.
- [67] <http://www.memsnet.org/material/silicondioxidesio2bulk/>
- [68] <http://www.siliconfareast.com/sio2si3n4.htm>
- [69] Melle, S.; De Conto, D.; Mazenq, L.; Dubuc, D.; Poussard, B.; Bordas, C.; Grenier, K.; Bary, L.; Vendier, O.; Muraro, J.L.; Cazaux, J.L.; Plana, R.; Failure predictive model of capacitive RF-MEMS, *Microelectronics Reliability*, 45, 1770 (2005)

- [70] J. Vandershueren and J. Casiot in: Braunlich P (Ed.) Topics in Applied Physics: *Thermally stimulated relaxation in solids*, vol. 37, ch.4, pp 135-223, Springer-Verlag, Berlin, (1979)
- [71] G. Papaioannou, J. Papapolymerou, P. Pons and R. Plana, *Appl. Phys. Letters* 90, 233507, (2007)
- [72] G. Papaioannou, F. Giacomozzi, E. Papandreou and B. Margesin, Proceedings of the 2007 MEMSWAVE Workshop, *8th International Symposium on RF MEMS and RF Microsystems*, Barcelona, Spain, (2007).
- [73] P.Czarnecki, X. Rottenberg, P. Soussan, P. Ekkels, P. Muller, P. Nolmans, W. De Raedt, H.A.C. Tilmans, R. Puers, L. Marchan³ and I. De Wolf, *Proceed. of MEMS2008 Conference* (2008).
- [74] Balaji Lakshminarayanan, Denis Mercier, and Gabriel M. Rebeiz, *IEEE Trans. on Microwave Theory and Tech.*, 56, 971 (2008).
- [75] S.P. Lau, J.M. Shannon and B.J. Sealy, *Journal of Non-Crystalline Solids* 277, 533, (1998)

IntechOpen



Microelectromechanical Systems and Devices

Edited by Dr Nazmul Islam

ISBN 978-953-51-0306-6

Hard cover, 480 pages

Publisher InTech

Published online 28, March, 2012

Published in print edition March, 2012

The advances of microelectromechanical systems (MEMS) and devices have been instrumental in the demonstration of new devices and applications, and even in the creation of new fields of research and development: bioMEMS, actuators, microfluidic devices, RF and optical MEMS. Experience indicates a need for MEMS book covering these materials as well as the most important process steps in bulk micro-machining and modeling. We are very pleased to present this book that contains 18 chapters, written by the experts in the field of MEMS. These chapters are grouped into four broad sections of BioMEMS Devices, MEMS characterization and micromachining, RF and Optical MEMS, and MEMS based Actuators. The book starts with the emerging field of bioMEMS, including MEMS coil for retinal prostheses, DNA extraction by micro/bio-fluidics devices and acoustic biosensors. MEMS characterization, micromachining, macromodels, RF and Optical MEMS switches are discussed in next sections. The book concludes with the emphasis on MEMS based actuators.

How to reference

In order to correctly reference this scholarly work, feel free to copy and paste the following:

Romolo Marcelli, Andrea Lucibello, Giorgio De Angelis, Emanuela Proietti, George Papaioannou, Giancarlo Bartolucci, Flavio Giacomozzi and Benno Margesin (2012). Characterization and Modeling of Charging Effects in Dielectrics for the Actuation of RF MEMS Ohmic Series and Capacitive Shunt Switches, Microelectromechanical Systems and Devices, Dr Nazmul Islam (Ed.), ISBN: 978-953-51-0306-6, InTech, Available from: <http://www.intechopen.com/books/microelectromechanical-systems-and-devices/characterization-and-modeling-of-charging-effects-in-dielectrics-for-the-actuation-of-rf-mems-ohmic->

INTECH
open science | open minds

InTech Europe

University Campus STeP Ri
Slavka Krautzeka 83/A
51000 Rijeka, Croatia
Phone: +385 (51) 770 447
Fax: +385 (51) 686 166
www.intechopen.com

InTech China

Unit 405, Office Block, Hotel Equatorial Shanghai
No.65, Yan An Road (West), Shanghai, 200040, China
中国上海市延安西路65号上海国际贵都大饭店办公楼405单元
Phone: +86-21-62489820
Fax: +86-21-62489821

© 2012 The Author(s). Licensee IntechOpen. This is an open access article distributed under the terms of the [Creative Commons Attribution 3.0 License](https://creativecommons.org/licenses/by/3.0/), which permits unrestricted use, distribution, and reproduction in any medium, provided the original work is properly cited.

IntechOpen

IntechOpen